University of Wollongong

Research Online

Faculty of Science, Medicine and Health - Papers: part A

Faculty of Science, Medicine and Health

1-1-2015

# An investigation into the interactions of gold nanoparticles and anti-arthritic drugs with macrophages, and their reactivity towards thioredoxin reductase

Lloyd James
*University of Wollongong*, lj521@uowmail.edu.au

Zhi-Qiang Xu
*University of Wollongong*, zhiqiang@uow.edu.au

Ronald Sluyter
*University of Wollongong*, rsluyter@uow.edu.au

Emma Hawksworth
*University of Wollongong*, elh994@uowmail.edu.au

Celine Kelso
*University of Wollongong*, celine@uow.edu.au

Follow this and additional works at: https://ro.uow.edu.au/smhpapers

*See next page for additional authors*

 Part of the Medicine and Health Sciences Commons, and the Social and Behavioral Sciences Commons

## Recommended Citation

James, Lloyd; Xu, Zhi-Qiang; Sluyter, Ronald; Hawksworth, Emma; Kelso, Celine; Lai, Barry; Paterson, David J.; de Jonge, Martin D.; Dixon, Nicholas E.; Beck, Jennifer; Ralph, Stephen F.; and Dillon, Carolyn T., "An investigation into the interactions of gold nanoparticles and anti-arthritic drugs with macrophages, and their reactivity towards thioredoxin reductase" (2015). *Faculty of Science, Medicine and Health - Papers: part A*. 2466.
https://ro.uow.edu.au/smhpapers/2466

Research Online is the open access institutional repository for the University of Wollongong. For further information contact the UOW Library: research-pubs@uow.edu.au

# An investigation into the interactions of gold nanoparticles and anti-arthritic drugs with macrophages, and their reactivity towards thioredoxin reductase


## Abstract

Gold(I) complexes are an important tool in the arsenal of established approaches for treating rheumatoid arthritis (RA), while some recent studies have suggested that gold nanoparticles (Au NPs) may also be therapeutically efficacious. These observations prompted the current biological studies involving gold(I) anti-RA agents and Au NPs, which are aimed towards improving our knowledge of how they work. The cytotoxicity of auranofin, aurothiomalate, aurothiosulfate and Au NPs towards RAW264.7 macrophages was evaluated using the MTT assay, with the former compound proving to be the most toxic. The extent of cellular uptake of the various gold agents was determined using graphite furnace atomic absorption spectrometry, while their distribution within macrophages was examined using microprobe synchrotron radiation X-ray fluorescence spectroscopy. The latter technique showed accumulation of gold in discrete regions of the cell, and co-localisation with sulfur in the case of cells treated with aurothiomalate or auranofin. Electrospray ionization mass spectrometry was used to characterize thioredoxin reductase (TrxR) in which the penultimate selenocysteine residue was replaced by cysteine. Mass spectra of solutions of TrxR and aurothiomalate, aurothiosulfate or auranofin showed complexes containing bare gold atoms bound to the protein, or protein adducts containing gold atoms retaining some of their initial ligands. These results support TrxR being an important target of gold(I) drugs used to treat RA, while the finding that Au NPs are incorporated into macrophages, but elicit little toxicity, indicates further exploration of their potential for treatment of RA is warranted.



## Disciplines

Medicine and Health Sciences | Social and Behavioral Sciences

## Publication Details

James, L. R. A., Xu, Z., Sluyter, R., Hawksworth, E. L., Kelso, C., Lai, B., Paterson, D. J., de Jonge, M. D., Dixon, N. E., Beck, J. L., Ralph, S. F. & Dillon, C. T. (2015). An investigation into the interactions of gold nanoparticles and anti-arthritic drugs with macrophages, and their reactivity towards thioredoxin reductase. Journal of Inorganic Biochemistry, 142 28-38.



## Authors

Lloyd James, Zhi-Qiang Xu, Ronald Sluyter, Emma Hawksworth, Celine Kelso, Barry Lai, David J. Paterson, Martin D. de Jonge, Nicholas E. Dixon, Jennifer Beck, Stephen F. Ralph, and Carolyn T. Dillon



This journal article is available at Research Online: https://ro.uow.edu.au/smhpapers/2466

**An investigation into the interactions of gold nanoparticles and anti-arthritic drugs with macrophages, and their reactivity towards thioredoxin reductase**

Lloyd R. A. James [a,b], Zhi-Qiang Xu [a,b], Ron Sluyter [a,c,d], Emma L. Hawksworth [a,b], Celine Kelso [a,b], Barry Lai [e], David J. Paterson [f], Martin D. de Jonge [f], Nicholas E. Dixon [a,b,d], Jennifer L. Beck [a,b], Stephen F. Ralph [a,b], Carolyn T. Dillon [a,b,d]*

[a] *Centre for Medical and Molecular Bioscience, University of Wollongong, NSW 2522, Australia.*

[b] *School of Chemistry, University of Wollongong, NSW 2522, Australia.*

[c] *School of Biological Sciences, University of Wollongong, NSW 2522, Australia.*

[d] *Illawarra Health and Medical Research Institute, Wollongong, NSW 2522, Australia.*

[e] *X-Ray Science Division, Advanced Photon Source, Argonne National Laboratory, Argonne, IL 60439, USA*

[f] *Australian Synchrotron, Clayton, VIC 3168, Australia.*

* Corresponding author. Tel.: +61 2 4221 4930; fax: +61 2 4221 4287.

*E-mail address:* carolynd@uow.edu.au

**Abstract:**

Gold(I) complexes are an important tool in the arsenal of established approaches for treating rheumatoid arthritis (RA), while some recent studies have suggested that gold nanoparticles (Au NPs) may also be therapeutically efficacious. These observations prompted the current biological studies involving gold(I) anti-RA agents and Au NPs, which are aimed towards improving our knowledge of how they work. The cytotoxicity of auranofin, aurothiomalate, aurothiosulfate and Au NPs towards RAW264.7 macrophages was evaluated using the MTT assay, with the former compound proving to be the most toxic. The extent of cellular uptake of the various gold agents was determined using graphite furnace atomic absorption spectrometry, while their distribution within macrophages was examined using microprobe synchrotron radiation X-ray fluorescence spectroscopy. The latter technique showed accumulation of gold in discrete regions of the cell, and co-localisation with sulfur in the case of cells treated with aurothiomalate or auranofin. Electrospray ionization mass spectrometry was used to characterize thioredoxin reductase (TrxR) in which the penultimate selenocysteine residue was replaced by cysteine. Mass spectra of solutions of TrxR and aurothiomalate, aurothiosulfate or auranofin showed complexes containing bare gold atoms bound to the protein, or protein adducts containing gold atoms retaining some of their initial ligands. These results support TrxR being an important target of gold(I) drugs used to treat RA, while the finding that Au NPs are incorporated into macrophages, but elicit little toxicity, indicates further exploration of their potential for treatment of RA is warranted.

*Keywords:*
Gold nanoparticles
Thioredoxin reductase
Macrophages
Rheumatoid arthritis
Gold complexes

## 1. Introduction

Chrysotherapy is the use of gold compounds for medical applications, foremost of which is the treatment of rheumatoid arthritis (RA). The use of gold compounds to treat RA dates back to pioneering studies by Forestier in the 1920s and 1930s [1–3]. Subsequently, for over 50 years, chrysotherapy became a mainstay of treatment for RA, with sodium aurothiomalate (Myochrisine), gold thioglucose (Solganol), sodium bis(thiosulfato)gold, and auranofin (Ridaura) among the most used therapeutic agents [4,5]. Each of these compounds contains gold in the +1 oxidation state (Fig. 1). Although their use has waned recently, chrysotherapy still remains an important chemotherapeutic approach to the treatment of RA.

Both aurothio-malate and -glucose are polymeric compounds containing Au(I) ions bound to two sulfur atoms. In contrast, sodium bis(thiosulfato)gold and auranofin are monomeric complexes in which the Au(I) center is bound to two sulfur atoms or a sulfur and a phosphorus, respectively. Auranofin entered clinical trials in the 1980s with much promise owing to its ability to be given to patients by oral administration. Nevertheless, the polymeric compounds are more effective treatments for RA than auranofin, although their use is associated with greater toxicity and unfavorable side effects [6].

Despite their long history of clinical use, the precise details of the mechanism(s) of action of chrysotherapeutic agents are not known. This is due in part to the complexity of the autoimmune response that is at the center of RA, and the wide range of biological targets *in vivo* [7]. For example, auranofin inhibits activation of the transcription protein complex NF-κB [8], and reduces expression of the inflammatory enzyme COX-2 [8,9]. Production of nitric oxide [10] and the pro-inflammatory cytokines TNF-α, IL-1β and IL-6 are also reduced by auranofin treatment [9,11], while aurothiomalate also inhibits production of TNF-α [12].

The Au(I) drugs are metabolized into their pharmacologically active forms after administration to patients. Initially the majority of the gold becomes bound to Cys-34 of serum albumin in processes that result in the loss of most, if not all, of the original ligands [4]. Several metabolites of the gold(I) complexes have been identified, including $[Au(CN)_2]^-$, Au(III) complexes and Au(0) [7]. It has also been shown that cells sequester gold into lysosomal bodies termed aurosomes [13,14]. X-ray absorption near edge spectroscopy (XANES) showed that aurosomal gold in the tissues of rats treated with aurothiomalate or $[AuCl_4]^-$ is present in the +1 oxidation state, while extended X-ray absorption fine structure (EXAFS) spectroscopy showed that the metal was bound to two sulfur atoms [15].

One mechanism by which the gold(I) drugs exert their anti-RA effects is inhibition of hydrolytic enzymes such as β-glucuronidase and elastase [5]. In addition, aurothiomalate and auranofin inhibit cathepsins K and S, which play a role in the progression of RA [16]. Thioredoxin reductase (TrxR) is another enzymatic target for metabolites of the gold drugs. This dimeric protein regulates cellular processes via reduction of thioredoxin (Trx) [17]. Both Trx and TrxR are over-expressed in synovial cells or fluid of RA patients [18,19]. Inhibition of TrxR by gold drugs has attracted interest due to the presence of a selenocysteine residue at its active site, and the greater affinity of Au(I) for selenol groups compared to thiols [20,21]. In addition, while platinum complexes bind to the active site of TrxR [22], some gold drugs inhibit the enzyme more potently [23–26]. Matrix assisted laser desorption/ionization mass spectrometry (MALDI-MS) showed that multiple molecules of gold compounds bind to TrxR [27], suggesting the presence of binding sites other than the active site selenocysteine. Several other mechanisms of anti-RA action have been proposed, including inhibition of leukocyte infiltration [28], modulation of the adhesion of polymorphonuclear neutrophils [29] and modification of macrophage activity [30]. It has also been suggested that various metabolites

of the Au(I) drugs modulate activity of the immune system by binding directly to T-cell receptors to block antigen signaling [31].

The formation of Au(III) and Au(0) metabolites from the Au(I) drugs suggests the latter undergo redox chemistry *in vivo* [32,33]. It has also been proposed that Au(0) is responsible for the anti-arthritic activity of Au(I) complexes, whilst Au(III) gives rise to the side-effects. Not surprisingly the anti-arthritic activity of gold nanoparticles (Au NPs) have been investigated in an effort to avoid side effects. In one study, rats that had been chemically induced to exhibit symptoms of inflammation were treated with either Au NPs or sodium aurothiomalate [34]. Those treated with Au NPs showed a greater reduction in the severity of symptoms, encouraging further investigations. One such study involved human patients with chronic RA that had proven unresponsive to other treatments. A significant reduction in the severity of symptoms was demonstrated in 9 of 10 patients [35]. Moreover, studies focusing on cell systems provided clues as to how Au NPs may elicit their anti-inflammatory activity. For example, they inhibit production of reactive nitrogen [36] and oxygen [37] species, as well as activation of NF-κB [36]. In addition, Au NPs do not induce secretion of the pro-inflammatory cytokines TNF-α and IL-1β [37].

Here we present the first systematic comparison of the cytotoxicity, uptake and cellular distribution of auranofin, sodium aurothiomalate and Au NPs with RAW264.7 macrophages. Macrophages are of particular interest in the study of RA, since they have been implicated in the pathogenesis of the disease [38–40]. In addition, we used electrospray ionization mass spectrometry (ESI-MS) to compare the binding of the gold drugs and Au NPs to a modified form of TrxR, containing an active site cysteine instead of selenocysteine.

## 2. Experimental

### *2.1. Materials*

All aqueous solutions were prepared using Milli-Q water (18.2 MΩ, Millipore). Sodium aurothiomalate, aurothioglucose, auranofin, gold(III) chloride (99.9%) and 3-(4,5-dimethylthiazol-2-yl)-2,5-diphenyltetrazolium bromide (MTT) were obtained from Sigma-Aldrich. Sodium aurothiosulfate was obtained from Alfa Aesar. Fetal bovine serum (FBS, heat-inactivated) was purchased from Bovogen Biologicals. GlutaMAX and Roswell Park Memorial Institute-1640 cell culture medium powder (RPMI-1640) were purchased from Life Technologies.

### *2.2. Synthesis of gold nanoparticles*

A stock solution of Au NPs was synthesized according to Turkevich et al. [41], with some modifications. Water (30 mL) was heated to near boiling, and a solution of $HAuCl_4$ (0.01 M in water, 2 mL) was added. This was followed by a solution of tri-sodium citrate (0.02 M, 4 mL), and the resulting red solution was heated for 1 h, cooled to room temperature, and then transferred to a volumetric flask (50.00 mL) to which water was added to produce a final concentration of 400 μM gold(0) atoms, assuming complete conversion of Au(III).

The Au NPs were characterized as follows. Absorption spectra were obtained using a Varian Cary 500 UV-VIS-NIR spectrophotometer equipped with quartz cuvettes. Particle size analysis was performed using a Malvern Zetasizer Nano S, while field emission scanning electron microscopy (FESEM) images were obtained using a JEOL JSM-7500FA instrument. The FESEM samples were prepared by allowing a small volume of the Au NP solution to evaporate on a carbon-copper film.

*2.3. Cell studies*

RAW264.7 macrophage cells were obtained as frozen permanents from the American Type Culture Collection (Manassas, VA) and were grown in RPMI-1640 medium containing 10% FBS and 1% v/v GlutaMAX at 37 °C and 5% $CO_2$. They were subcultured at 90% confluence. Treatment solutions of sodium aurothiomalate or sodium aurothiosulfate were prepared in RPMI-1640 medium containing 1% v/v GlutaMAX (RPMI-GlutaMAX medium). Control cells were also treated with RPMI-GlutaMAX medium. In contrast, treatment solutions containing auranofin were prepared in 1% v/v DMSO in RPMI-GlutaMAX medium. Treatment solutions of Au NPs were prepared in water and diluted to 15% v/v water in 85% RPMI-GlutaMAX medium. Trypan blue assays were used to assess the number of viable cells by adding 50 μL of cell suspension to 50 μL of trypan blue solution (0.5% w/v in phosphate buffered saline (PBS), Sigma-Aldrich). The number of cells was scored using a hemocytometer and a light microscope at 10× magnification. Cells that excluded the dye (uncompromised membrane integrity) were assumed to be 'healthy/viable' while those that stained blue were classified as 'dead/non-viable.'

*2.4 MTT assays*

Cytotoxicity of the gold compounds was assessed using the MTT assay. RAW264.7 cells ($5\times10^4$ in 100 μL) were seeded into each well of a 96-well plate and incubated overnight (37 °C, 5% $CO_2$). The medium was removed and the cells were washed twice with RPMI-GlutaMAX (300 μL). Freshly prepared treatment solutions containing the Au compounds or Au NPs at the required concentrations were added to the wells and incubated for 24 h. At the end of this period, the treatment solutions were removed and the adherent cells washed twice with RPMI-GlutaMAX (300 μL), before a further 100 μL of RPMI-GlutaMAX was added. In addition, MTT (50 μL, 2 mg/mL in PBS) was added and the plate was incubated for 4 h. This

solution was carefully removed and the resulting purple crystals were dissolved in DMSO (200 µL/well). The $A_{570}$ and $A_{630}$ were then measured using a BMG Labtech POLARstar Omega microplate reader. The $A_{630}$ value was used as a background reading, whilst the absorbance at 570 nm arose from the purple MTT dye in DMSO. Cell viabilities were calculated using equation 1.

**Equation 1:** $$\text{Cell Viability (\%)} = \frac{A570 - A630 \text{ (treated cells)}}{A570 - A630 \text{ (control cells)}} \times 100$$

Each plate contained 6 wells for each concentration of Au(I) compound or Au NPs, and 18 control wells. Each experiment was performed three times, and the errors are reported as the standard deviation of the mean.

*2.5. Graphite furnace atomic absorption spectroscopy (GFAAS)*

RAW264.7 cells ($5\times10^6$ in 5 mL growth medium) were seeded into a sterile 60-mm cell culture dish and incubated for 24 h. The medium was then removed and the cells were washed once with PBS and once with RPMI-GlutaMAX. Treatment solutions containing the Au compounds or Au NPs were then added to the cells, which were then incubated for 24 h. The treatment solutions were collected in a centrifuge tube. RPMI-GlutaMAX (5 mL) was added to the dish and the cells were harvested. This suspension was combined with the initial treatment solution and both were centrifuged (300×*g*, 5 min). The supernatant was removed and the cells were resuspended in 5 mL of RPMI-GlutaMAX and re-centrifuged (300×*g*, 5 min). This was repeated, after which the final pellet was resuspended in 1 mL of RPMI-GlutaMAX. A small aliquot (50 µL) was removed and the numbers of viable and dead cells in each sample were determined using the trypan blue assay. The remainder of the cells were centrifuged and washed twice with a saline solution (0.9% w/v). The pellets were freeze-dried for 2 h and digested in 10–100 µL of nitric acid (Ultrapur, Merck Millipore, 60% v/v)

overnight, depending on the sample (cell density and treatment concentration). The resulting solutions were subsequently diluted in 5.00 or 50.00 mL volumetric flasks containing a final nitric acid concentration of 0.6% v/v. Triplicate cell samples were prepared following treatment with each concentration of Au(I) compound or Au NPs.

GFAAS measurements of the final solutions used a PerkinElmer AAnalyst 600 atomic absorption spectrometer equipped with the Winlab 32 AA Furnace program, incorporating Zeeman-effect background correction, an AS-800 autosampler and an AA Accessory cooling system. A gold hollow cathode lamp (PerkinElmer) was employed at a wavelength of 242.8 nm with a slit width of 0.7 nm, to give an instrument energy reading of approximately 50 W. A certified Au standard solution (997 mg/L Au, 10% v/v HCl, PerkinElmer) was used to prepare the stock Au standard solution (50 μg/L, 0.6% v/v $HNO_3$) for the calibration curve (correlation coefficients: 0.994 and 0.992). The analyte (20 μL) was mixed with 5 μL of matrix modifier solution and atomized from the surface of a pyrolytic graphite-coated tube using the furnace operating conditions described in Table S1 (supporting data). Argon gas was used throughout the analysis, with absorption measurements conducted during the atomization stage (1800 °C). Triplicate measurements were performed for each sample.

*2.6. Microprobe synchrotron radiation X-ray fluorescence (SR-XRF) imaging*

The distributions of Au and other elements within macrophages that had been treated with either Au(I) compounds or Au NPs were determined by microprobe SR-XRF imaging. High spatial resolution imaging of single macrophages was performed at the Advanced Photon Source (APS), Argonne National Laboratory (Chicago, USA) while low spatial resolution imaging over a larger sample area was undertaken at the Australian Synchrotron (AS, Clayton, Australia). In both cases the samples were prepared on $Si_3N_4$ membranes (Silson, UK), which were initially washed once with ethanol (70% v/v), twice with sterile

PBS, and finally in cell growth medium, before being placed in a 60 mm cell culture dish. RAW 264.7 cells ($5\times10^6$ in 5 mL growth medium) were seeded into the dishes, which were then incubated (37 °C, 5% $CO_2$) overnight. After confirming that the cells had grown to a sufficient confluency on the $Si_3N_4$ membranes, the growth medium was removed and the cells were washed twice with RPMI-GlutaMAX to remove the FBS. Treatment solutions (5 mL), containing the appropriate concentrations of Au(I) compounds or Au NPs were then added prior to incubation for 24 h. Following this, the membranes were removed from the dish and washed by sequentially dipping in two solutions of PBS and then three solutions of 200 μM ammonium acetate. The cells were finally fixed by dipping once in methanol. The membranes were then stored in a desiccator until analysed.

Microprobe SR-XRF analysis of individual cells used the 2-ID-D beamline at APS with a monochromatic 13.45 keV X-ray beam focused to 0.3 $\mu m^2$ using two stacked zone plates. The $Si_3N_4$ membranes were mounted on a high precision XYZ motorized stage (PM20076), and the X-ray fluorescence detected using a Vortex EM (Radiant Detector Technologies, LLC 165-VTX-EM) silicon drift detector operating in fluorescence mode. High-resolution elemental maps were acquired over the scan areas specified in the figure captions using a 0.5 μm step size and 0.5 s/point dwell time. The elements were quantified with the aid of measurements from the thin film standards NBS-1832 and NBS-1833, obtained from the National Bureau of Standards (Gaithersburg, MD).

Elemental mapping of larger cell areas was carried out at the XFM beamline [42] at the AS using a monochromatic 12.055 keV X-ray beam focused to 2 μm in the horizontal and vertical dimensions using a Kirk-Patrick Baez mirror and a silicon drift diode detector operating in fluorescence mode. Elemental maps were acquired over 120 × 120 $\mu m^2$ areas using a 2 μm step size and 1 s/point dwell time. In both cases, the full fluorescence spectra

were fit to modified Gaussians and the data were processed using the MAPS software package, version 1.7.1.03, provided by Dr Stefan Vogt at APS.

*2.7. Expression and purification of TrxR*

A plasmid containing human thioredoxin reductase (TrxR), pET46-$(His)_6$-hTrxR1, was obtained from A. Wang [22]. The expressed protein had the codon for selenocysteine-498 mutated to a cysteine to facilitate bacterial expression and contained an N-terminal $His_6$ tag to assist purification. *E. coli* BL21(λDE3)/pLysS containing the $TRXR^+$ plasmid was grown in LB medium (750 mL) at 37 °C to $A_{600}$ = 0.6. The culture was cooled to 23 °C, and TrxR production was induced with 1 mM IPTG (isopropyl-β-D-thiogalactoside) overnight. Cells were collected by centrifugation (10000×*g*, 15 min) and resuspended in buffer A (50 mM Tris-HCl, pH 8.0, 500 mM NaCl, 10 mM imidazole), before being lysed using a French press. The lysate was clarified (28000×*g*, 30 min) and the supernatant loaded onto a $Ni^{2+}$-affinity column (HisTrap HP, GE Healthcare). The column was eluted with 12 mL of 25 mM imidazole, followed by a linear gradient (30 mL) of 25–350 mM imidazole in buffer A. Fractions containing the most pure TrxR, as assessed by SDS-PAGE were combined, dialyzed into buffer B (30 mM Tris-HCl, pH 8.0, 2 mM dithiothreitol, 1 mM EDTA), and loaded onto an anion-exchange column (8-mL MonoQ GL, GE Healthcare). Purified TrxR was eluted with 12 mL of 120 mM NaCl followed by a linear gradient (160 mL) of 120–300 mM NaCl in buffer B. Fractions containing ≥90% purified TrxR were pooled, frozen in liquid nitrogen and stored at –80 °C.

*2.8. Electrospray ionization mass spectrometry (ESI-MS)*

TrxR (200 μL) was dialyzed at 4 °C against either 0.1 or 0.5 M ammonium acetate, pH 7.2 containing 1 mM dithiothreitol, and then twice (3 h each) against the same solutions without dithiothreitol. The protein concentration was determined from $A_{280}$. Stock solutions of

each Au complex were prepared freshly, and the calculated volumes added to give reaction mixtures containing the desired concentration of gold drug. After storage of the mixtures on ice, glacial acetic acid was added to 5% (v/v). The mixtures were then immediately analyzed using ESI-MS. Spectra were acquired using a Waters (Manchester, UK) Q-ToF Ultima ESI mass spectrometer operating in positive ion mode using a nanospray source, over the *m/z* range 1000–6500, with at least 50 acquisitions combined to give the final spectrum. The instrument was calibrated using a 10 mg/mL caesium iodide solution in 70% isopropanol/ water. Raw spectra were background subtracted and smoothed using the Savitsky-Golay algorithm, and the charge series ions transformed to mass scale using MassLynx software. Stated masses and their errors were calculated using MassLynx software.

## 3. Results and discussion

### *3.1 Characterization of gold nanoparticles*

Au NPs were characterized by absorption spectrophotometry, field emission scanning electron microscopy (FESEM) and particle size analysis. The UV-vis absorption spectrum (supplementary data, Fig. S1) showed one broad peak centered at 522 nm, consistent with the plasmon resonance band observed in other samples of gold nanoparticles [43]. FESEM indicated that the particles were spherical in shape and relatively uniform in size, ranging from 10–20 nm in diameter (supplementary data, Fig. S2). Similarly, particle size analysis showed the average diameter of the Au NPs to be 23 ± 7 nm.

### *3.2 Cytotoxicity studies*

Auranofin exhibited significant cytotoxicity against the RAW264.7 macrophages, resulting in an $IC_{50}$ of 4 μM (Fig. 2). This value is consistent with previous investigations of the toxicity of this drug, where auranofin was found to have an $IC_{50}$ of 1.5 μM against a B16 mouse melanoma cell line using a clonogenic assay [44], and an $IC_{50}$ of 1.06 μM against a human ovarian cancer cell line using a 24 h MTT assay [45]. In contrast, Au NPs were non-toxic over the concentration range 0.1–60 μM (Fig. 2). Higher concentrations of NPs could not be tested as these would have resulted in hypotonic conditions due to excess diluent. The lack of cytotoxicity induced by Au NPs is consistent with a report by Shukla et al. [37], who observed only minor decreases in cell viability (as assessed by the MTT assay) when macrophages were treated with 10–100 μM Au NPs for 24 h.

Aurothiomalate was also non-toxic towards the macrophage cells at all concentrations examined in the current study (up to 1 mM). This contrasts with a previous report that showed it exhibited an $IC_{50}$ of 60 μM against the B16 mouse melanoma cell line. It is important to

note, however, that the latter study used a clonogenic assay [44]. Therefore the observed toxicity may have been due to the drug having a degree of specificity for the melanoma cell line. Consistent with this is the observation of negligible toxicity of aurothiomalate towards a human umbilical vein endothelial (HUVE) cell line using both a $^{51}Cr$ release assay and an MTT assay [28].

Aurothiosulfate was more toxic than aurothiomalate, but far less toxic than auranofin, with an $IC_{50}$ of 650 μM. The low cytotoxicity of aurothiosulfate is consistent with the results of a prior study in which the MTT assay was used to measure its effects on human THP1 monocytes; no cytotoxicity was observed with 5 μM aurothiosulfate [46].

*3.2 Cellular gold uptake*

A fundamental question that arises from these data is whether the observed variations in cell toxicity stem primarily from differences in cellular uptake of the gold complexes and NPs. To address this question, GFAAS was used to determine the extent of uptake of Au by RAW264.7 macrophages exposed for 24 h to Au NPs, aurothiosulfate or aurothiomalate at either 2.5 or 60 μM, to provide a direct comparison of the extent of uptake. Experiments with auranofin used the drug only at 2.5 μM since higher concentrations resulted in cell death (Fig. 2). The results of these experiments, together with those obtained from cell viability experiments using the trypan blue assay under similar conditions are shown in Fig. 3.

The trypan blue experiments (Fig. 3a) confirmed that the vast majority of the cells exposed to Au NPs, aurothiosulfate or aurothiomalate remained viable with intact membranes. Only in the case of cells exposed to auranofin were the percentages of viable and non-viable cells roughly equivalent (40% non-viable), which correlates with the results of the

MTT assay. This also supports the hypothesis that the measured levels of gold uptake for all compounds and NPs examined, with the exception of auranofin, was due to their ability to enter the cells, and not due to breakdown of the cellular membrane subsequently allowing passage of gold.

Comparison of the uptake data following exposure of the cells to each of the gold complexes and Au NPs at a concentration of 2.5 μM Au (Fig. 3b) revealed that only the NPs and auranofin showed statistically significant uptake of gold in comparison to control cells ($P$ <0.001). The capacity for macrophages to incorporate auranofin is not surprising, given that this complex has a distinctly different structure to aurothiomalate and aurothiosulfate. Auranofin has a lipophilic structure that facilitates its transport across cell membranes [47], and therefore contributes to its higher cytotoxicity. Conversely, the lower cytotoxicity of aurothiomalate and aurothiosulfate at 2.5 μM may be due to their relative inability to enter macrophages; very low amounts of gold were incorporated into the macrophages after exposure to these two compounds.

Differences in the amount of gold uptake by cells were more substantial following exposure to higher Au concentrations. For example, significant ($P$ <0.001) uptake was observed for cells exposed to 60 μM aurothiomalate, aurothiosulfate or Au NPs. In the case of aurothiomalate an ~70-fold increase in the uptake of Au, from $7.6\times10^{-15}$ to $5.2\times10^{-13}$ g/cell, occurred as a result of increasing the concentration of drug from 2.5 to 60 μM. An even more substantial increase in the level of gold uptake (to $1.4\times10^{-12}$ g/cell) was observed following treatment with 60 μM aurothiosulfate. This is 100 times the value of $1.4\times10^{-14}$ g/cell obtained when the cells were exposed to 2.5 μM aurothiosulfate.

Exposure to 60 μM Au NPs resulted in the greatest cellular gold uptake, ($P$ <0.001 in comparison to aurothiosulfate and aurothiomalate), and a 33-fold increase in the amount of

gold incorporated into the macrophages when compared to cells treated with 2.5 μM Au NPs ($9.7\times10^{-14}$ to $3.3\times10^{-12}$ g/cell). Chithrani et al. [48] have shown that gold nanoparticles can enter cells via a receptor-mediated, clathrin-dependent endocytosis pathway. Furthermore the uptake half-life varies with size, with smaller nanoparticles taken up the fastest ($t_{½}$ = 1.9–2.2 h) [49]. By comparison, it has been reported that auranofin enters cells by the sulfhydryl shuttle model, where the $Au(PEt)_3^+$ fragment binds to a membrane transport protein through a thiol group and is subsequently transported through the membrane [50]. It is possible that the other gold(I) drugs follow a similar mechanism, and thus may partially explain why Au NPs are taken up in more significant quantities. Importantly, there was no evidence of toxicity at 60 μM Au for aurothiomalate, aurothiosulfate or Au NPs as determined by the MTT assay (Fig. 2). If the extent of cytotoxicity were related primarily to the amount of intracellular gold, one would expect that the toxicity would increase in the order: aurothiomalate < aurothiosulfate < Au NPs. Whilst Fig. 2 shows that aurothiosulfate is more cytotoxic than aurothiomalate, it was not possible to determine whether or not Au NPs were more toxic than either or both of these gold complexes owing to the restricted range of concentrations of Au NPs that could be used.

*3.3 Cellular Au distribution*

Microprobe SR-XRF was used to image gold in single cells and small clusters of RAW264.7 macrophages after exposure to different concentrations of aurothiomalate, auranofin or Au NPs for 24 h. The results of these experiments are presented as elemental distribution maps for individual elements in Fig. 4. Macrophages were either treated with treatment medium, 1000 μM sodium aurothiomalate, 2.5 μM auranofin or 60 μM Au NPs. The low count and random distribution of gold in the control cells (Fig. 4a) is essentially background noise associated with the very low concentration of this element. This indicates

that the gold present in the remaining cells originated from treatment with the gold complexes or Au NPs.

All three samples exposed to gold complexes or Au NPs show a high degree of co-localization of gold with sulfur. The most likely explanation for this observation, in the case of sodium aurothiomalate and auranofin, is that the gold has become associated with sulfur that is endogenous to the cell, in the form of thiol-containing species such as glutathione or proteins. It is also theoretically possible that sulfur was observed to be co-localized with gold after the macrophages were treated with sodium aurothiomalate, simply because both elements are present in this compound. However, this explanation is extremely unlikely, since it has been reported that the original sulfur-donor ligands associated with the gold complexes undergo ligand exchange reactions when the complexes are introduced into biological systems (discussed further in Section 3.4) [47]. In addition, the results of the mass spectrometry studies presented in Section 3.4 also reveal rapid loss of the S-containing ligands from the Au coordination sphere in the complexes under study.

The microprobe SR-XRF observation of co-localization between Au and S in cells treated with Au NPs, however, stems from issues inherent to the detection method that occur as a result of the dominating Au M line. Inspection of the spectra of the characteristic X-ray lines (Fig. S3) reveals that the Au M line (2.1 keV) is in close proximity to the P (2.0 and 2.1 keV) and S (2.3 and 2.4 keV) K lines. In the case of cells treated with the Au NPs, the Au-M line is so significant that it dominates the region to the extent that it encroaches on the P and S K lines, thereby contributing to the intensity of the latter signals. In contrast, the Au M line was less intense following treatment with aurothiomalate and auranofin, due to the lower level of Au uptake by the cells. This supports the conclusion that co-localization in the case of macrophages treated with the Au complexes was due to interactions between gold and sulfur, most likely inside the cells.

In addition, it is apparent that the gold distribution differs according to treatment and physical appearance of the cells. For instance, in the top left and bottom right auranofin-treated cells in Fig. 4c, the Au is distributed throughout the entire cell. However, this is not the case for the more fibroblastic cell located diagonally in the image. The fact that the uptake is greater in the rounder cells is consistent with the cells dying and losing membrane integrity. In contrast, the cells treated with aurothiomalate and Au NPs (Fig. 4b and 4d) show more discrete/localized areas of Au and there is evidence of co-localization of Au with Ca, Zn and Cu.

The GFAAS data (Fig. 3) indicate that Au NPs were taken up by the macrophages to an extent greater, at least by an order of magnitude, than either of the clinically used gold drugs. The presence of discrete hotspots corresponding to gold in macrophages treated with Au NPs is consistent with earlier work that used transmission electron microscopy to show that Au NPs were packaged into endosomes and then lysosomes following entry into the cells [51]. It is likely that the same events occur in macrophages following treatment with aurothiomalate [13,14].

Fig. 5 shows the elemental distribution maps for large numbers of macrophages exposed to treatment medium only, or to 1000 μM aurothiomalate, 2.5 μM auranofin or 60 μM Au NPs. These results allow comparisons to be made regarding the homogeneity of gold uptake across the cell population. Spectra of the characteristic X-ray lines for these maps are shown in Fig. S4. Treatment with aurothiomalate led to a sparse pattern of gold uptake, with the majority of cells exhibiting regions of low gold intensity that were comparable with the background. Despite this, some regions of the gold map feature ‘hot spots’ of gold that are associated with cellular material. Similarly, macrophages exposed to auranofin exhibit a non-uniform distribution of gold, with some cells showing much greater uptake than others, as is consistent with the results shown in Fig. 4c. Close examination of cells that displayed the

greatest uptake of auranofin showed they had a more rounded morphology than those that had incorporated less gold. This observation is consistent with changes in cell morphology noted previously for RAW264.7 macrophages that had been exposed to acute cytotoxic agents [52].

Macrophages exposed to Au NPs showed the most homogeneous pattern of gold incorporation of any of the samples studied, with the majority displaying significant levels of uptake. This is consistent with the GFAAS results (Fig. 3), which showed higher levels of gold incorporation into Au NP-treated cells, and supports the suggestion that the Au NPs experience a wider range of biochemical interactions inside cells compared to the discrete gold complexes.

*3.4 Thioredoxin reductase binding studies*

The enzyme TrxR is attracting growing interest as a target for a variety of metallodrugs [22,27,53]. Both X-ray crystallography and MALDI-MS were used previously to show that several terpyridineplatinum(II) complexes bind to TrxR [22], while various gold complexes have also proven to be potent inhibitors of this enzyme [24–26]. In addition, TrxR is involved in the redox activity of RAW264.7 macrophages [54–56]. Our interest in examining the binding of gold complexes, and possibly Au NPs, to TrxR was derived in part from the contribution that these interactions may make to their anti-arthritic activity [18,19]. In addition, it has been speculated that the anti-cancer activity of auranofin may be linked to its ability to interact with TrxR [45,57]. Further interest in examining the binding of the various gold agents to this protein stems from the reported use of MALDI-MS to examine the binding interactions between TrxR and several different Au(I) complexes, including auranofin, aurothiomalate and $AuPEt_3Cl$ [27]. As the MALDI-MS spectra obtained were very broad, it was not possible to accurately determine the exact number of gold molecules that had bound to the protein. Furthermore, the question of whether or not any of the ligands

initially bound to gold in the drugs had been retained upon binding to the protein could not be answered. ESI-MS has previously been used to investigate the binding of several gold compounds, including those with anti-arthritic activity, to human serum albumin [58,59]. It offers a number of advantages for studies of this type, since it enables determination of the stoichiometry of bound metal compounds.

Recombinant $His_6$-tagged human TrxR [22] was expressed in *E. coli* and purified using metal affinity and anion exchange chromatography. Because bacterial systems do not efficiently express selenoproteins, the penultimate selenocysteine residue was replaced by cysteine. Initial experiments focused on determining the best solution conditions for obtaining ESI mass spectra of the monomeric and dimeric forms of TrxR. All spectra were obtained using solutions of the protein that also contained aqueous ammonium acetate to facilitate formation of charged ions. Fig. 6a shows the positive ion ESI mass spectrum of TrxR obtained in a solution of 100 mM ammonium acetate and 5% acetic acid (pH 3.7). Several distinct envelopes of ions are apparent. Those with an $m/z \leq 3200$ are relatively narrow, and arise from the monomeric form of the protein. For example, the ion at $m/z$ 2682 corresponds to $[TrxR + 23H]^{23+}$. At higher $m/z$ values, envelopes of broader ions are also apparent that are attributable to TrxR dimers. For example, $m/z$ ~4932 is $[2TrxR + 23H]^{23+}$. Therefore both forms of the protein were present under these solution conditions. The presence of differing envelopes of ions for the monomer and dimer suggests populations of molecules that were unfolded to varying extents [60]. The observation of relatively narrow ions attributable to the monomeric form of the protein (width at half height ~2.5 Th) allows more information to be obtained from gold binding studies because it is possible to distinguish ions differing by only 10 Th; e.g., free protein molecules and protein molecules with a single bound gold ion.

Fig. 6b shows the positive ion ESI mass spectrum obtained using a solution containing a higher ammonium acetate concentration (500 mM, pH 7.2) and no acetic acid. Only a small

number of relatively broad peaks were observed. Although the *m*/*z* of these ions were different to any of those present in Fig. 6a, they were still from the dimeric form of the protein. For example, the ion at *m*/*z* ~4999 is from $[2\text{TrxR} + 23\text{H}]^{23+}$. This shows that the higher ammonium acetate concentration stabilized the protein in its dimeric form. Addition of acetic acid, even up to a concentration of 10%, failed to alter the appearance of the mass spectrum significantly. The broadness of the peaks in Fig. 6b prevented identification of ions arising from discrete gold/protein complexes in gold binding experiments. Therefore our efforts concentrated on examining the binding of the gold complexes and Au NPs to TrxR using conditions where the ESI mass spectrum gave ions of high abundance from the monomeric form of the protein, but where the reaction conditions had a mix of monomer and dimer present.

Fig. 7a shows the ESI mass spectrum of a 1.1 μM solution of TrxR after transformation to an absolute mass scale. The spectrum was obtained using the conditions in Fig. 6a. The mass of the protein calculated using its amino acid sequence is 56288 Da without the initiating methionine residue. The mass determined from the spectrum was in good agreement (56310 Da) given the errors associated with mass detection under these conditions [60]. Also present in the spectrum are ions of lower abundance at 56488 and 56529 Da. To date we have been unable to definitively assign these peaks to specific amino acid or post-translational modifications of TrxR. However, the peak at 56488 Da may be the result of the presence of the N-formyl-methionine (residue mass 169 Da) that initiates protein translation in *E. coli* [61]. Both peaks are likely due to covalently modified forms of the protein, as dialysis against formic acid instead of ammonium acetate resulted in no change to the ESI mass spectrum.

Also shown in Fig. 7 are ESI mass spectra of solutions containing various ratios of gold complexes and TrxR. Each of these shows ions attributable to protein molecules

containing different numbers of bare gold atoms. For example, the spectrum of a solution containing a 3:1 ratio of sodium aurothiosulfate and TrxR (Fig. 7b) showed ions from TrxR adducts containing between one and seven gold atoms, with those protein molecules having one, two or three bound gold atoms the most abundant. Ions attributable to protein adducts in which $[Au(S_2O_3)]^-$ moieties were bound to the protein were also present, but at much lower abundance, which is not surprising as it has been reported previously that gold complexes such as the chrysotherapeutic agents readily undergo ligand substitution reactions upon entering cells [4]. It is worth noting, however, that in an earlier study the most abundant ions present in the ESI mass spectrum of a solution containing a 0.5:1 ratio of aurothiosulfate and human serum albumin (HSA) were attributable to protein adducts containing one or two bound $Au(S_2O_3)$ moieties [59]. At present we are uncertain of the reasons for the variation in abundance of ions featuring $Au(S_2O_3)$ moieties bound to TrxR and HSA; they may be related to differences in instrumental parameters.

The spectrum of a solution containing a 3:1 ratio of sodium aurothioglucose and TrxR (Fig. 7c) contains ions which most likely arise from protein complexes containing between one and six gold atoms. However, making definitive assignments for some of these ions is extremely difficult owing to the similarities between the molecular weight of thioglucose (ca. 195) and the atomic weight of a single gold atom (196.97). This means, for example, that the ions at 56680 Da may be due to TrxR molecules with two bare gold atoms bound, protein molecules containing a single aurothioglucose moiety, or a mixture of both types of adducts. In considering this issue, it is worth noting that the spectrum of a solution containing TrxR and aurothiosulfate (Fig. 7b) contained many types of ions that could be unambiguously assigned to protein adducts containing different numbers of bound gold atoms. It is therefore reasonable to expect that coordination of the closely related aurothioglucose molecule to

TrxR would also occur concomitantly with cleavage of Au–S bonds and displacement of the original ligands present in the coordination sphere of the metal ion.

The spectrum of the solution containing a 5:1 ratio of auranofin and TrxR (Fig. 7d) contained ions attributable to adducts with one or more $AuPEt_3$ moieties bound to the protein, sometimes in addition to bare gold ions. These results may be compared to those from our previous MS investigation of the interactions of HSA with $AuPEt_3Cl$, a model for auranofin [59]. Each of the adducts observed consisted of protein molecules bound to one or more $AuPEt_3$ moieties. For TrxR, the most abundant ions were those attributable to protein molecules with one $AuPEt_3$ bound, while ions from protein molecules with two bound $AuPEt_3$ groups were of medium abundance (Fig. 7d). Thus, the Au–P bonds in auranofin and $AuPEt_3Cl$ remain largely intact upon coordination of the metal complex to TrxR or HSA and these bonds are stable under ESI conditions.

The observation of a high degree of Au NP uptake by macrophages prompted us to investigate whether or not they can bind directly to TrxR, as formation of such protein adducts might account at least partially for the observed anti-arthritic activity of Au NPs. However, treatment of TrxR with up to 5 equivalents of Au NPs for as long as 24 h failed to produce any new ions in ESI mass spectra. There are several possible reasons for this outcome, including that the Au(0) atoms present in Au NPs are unlikely to form bonds with the protein that are sufficiently stable to survive the ESI process, or alternatively, the size of the nanoparticles may prevent them from approaching cysteine residues exposed on the surface of the protein.

Interest in the environmental consequences of Au NPs, and their biomedical applications, has led to a number of reports on their interactions with proteins. One of the earliest such studies used zeta potential and quartz crystal microbalance techniques to

examine the binding of Au NPs to bovine serum albumin [62]. It was tentatively concluded that electrostatic forces, possibly involving the carboxylate groups of citrate anions on the surfaces of the Au NPs, and protonated amines of surface lysine residues of the protein, were responsible for the interactions. In a separate study, a combination of techniques, including circular dichroism spectroscopy and dynamic light scattering, was used to perform measurements on systems containing citrate-stabilized Au NPs of various sizes, and a range of proteins found in human blood [63]. The results of these investigations pointed to a model in which the proteins formed an outer layer, or "corona" on the surface of the Au NPs, and suggested that the overall strength of the interactions increased along with nanoparticle size. Binding constants ranging from $10^4$ to $10^7$ $M^{-1}$ were obtained for these systems, indicating that in some instances the overall strength of the binding interactions was quite low.

Evidence of interactions between thioredoxin reductase and nanoclusters composed of 25 gold atoms stabilized by a tridecapeptide has also been reported [64]. The positively charged peptide enhanced the solubility of the gold clusters, and also facilitated electrostatic binding interactions with a number of negatively charged amino acid residues near the active site of the enzyme. Molecular docking studies and molecular dynamics simulations were used to further probe the nature of the binding interactions, and demonstrate the stability of the resulting assembly. It was also shown that the gold nanoclusters inhibit the activity of TrxR, leading to higher levels of reactive oxygen species and apoptosis in HeLa cells. Silver nanoparticles have also been reported to inhibit selenoprotein synthesis, and the activity of TrxR in in vitro studies, resulting in an increase in oxidative stress [65].

The above studies highlight the ability of Au NPs or nanoclusters, or nanoparticles composed of other metals, to interact with proteins, including TrxR. Each of the techniques used in these investigations is non-destructive, and inherently well suited for probing weak binding interactions between two molecules. In contrast, whilst ESI-MS is known to employ

one of the “softer” ionization methods for obtaining mass spectra, the ability of non-covalent assemblies of molecules to be analyzed by this technique does vary widely owing to their exposure to high electrical potentials and moderately high temperatures. It is therefore likely that electrostatic interactions were taking place between the Au NPs and TrxR in samples prepared for mass spectrometry, but that these did not survive the conditions inside the spectrometer.

## 4. Conclusions

This work shows that exposure of macrophages to Au NPs, compared with Au(I) complexes that include chrysotherapeutic agents, results in significantly greater uptake of gold. In addition, Au NPs were hardly cytotoxic towards macrophages, and were significantly less toxic than auranofin. These results support the need to further explore the potential of Au NPs as anti-RA agents. Nevertheless, ESI-MS did not show evidence that AuNPs could interact with TrxR in the same manner as gold(I) complexes. Unfortunately the intense Au M-line in the microprobe SR-XRF spectrum means that it is impossible to determine whether gold derived from Au NPs co-localizes with sulfur. However, the gold maps highlighted that the nanoparticles most likely enter macrophages and become localized as discrete hot spots, suggesting that they are packaged into lysosomes as a detoxification mechanism. Our current work is focused on further elucidation of the mechanism(s) by which Au NPs may elicit an anti-RA response in patients.

## 5. Abbreviations

| | |
|---|---|
| APS | Advanced Photon Source |
| AS | Australian Synchrotron |
| Au NPs | gold nanoparticles |
| ESI-MS | electrospray ionization mass spectrometry |
| EXAFS | extended X-ray absorption fine structure |
| FBS | fetal bovine serum |
| FESEM | field emission scanning electron microscopy |
| GFAAS | graphite furnace atomic absorption spectroscopy |
| HSA | human serum albumin |
| HUVE | human umbilical vein endothelial |
| IPTG | isopropyl-β-D-thiogalactoside |

| | |
|---|---|
| MALDI-MS | matrix assisted laser desorption/ionization mass spectrometry |
| MTT | 3-(4,5-dimethylthiazol-2-yl)-2,5-diphenyltetrazolium bromide |
| PBS | phosphate buffered saline |
| Q-ToF | quadrupole time-of-flight |
| RA | rheumatoid arthritis |
| RPMI-1640 | Roswell Park Memorial Institute-1640 |
| SR-XRF | Synchrotron radiation X-ray fluorescence |
| TrxR | thioredoxin reductase |
| TNF-α | tumor necrosis factor alpha |
| XANES | X-ray absorption near edge spectroscopy |

**Acknowledgments**

The use of the XFM beamline at the Australian Synchrotron was supported by that facility. Use of APS was supported by the U.S. Department of Energy Office of Science under Contract No. DE-AC02-06CH11357. CTD acknowledges travel funding provided by the International Synchrotron Access Program managed by the Australian Synchrotron. The authors acknowledge the Australian Research Council and the University of Wollongong for the mass spectrometers used in this work (Q-ToF Ultima, LIEF grant LE0453832), and thank Tony Romeo for performing the FESEM and Yan-Chung Lo and Andrew Wang (Academia Sinica, Taiwan) for the TrxR plasmid. LRAJ was supported by an Australian Postgraduate Award.

## References


[1] J. Forestier, Bull. Mem. la Soc. Medicale des Hop. Paris 53 (1929) 323–327.

[2] J. Forestier, Ann. Med. Interne (Paris) 53 (1929) 232–237.

[3] J. Forestier, M. Paris, Lancet 219 (1932) 441–444.

[4] C.F. Shaw, Chem. Rev. 99 (1999) 2589–2600.

[5] W.F. Kean, I.R.L. Kean, Inflammopharmacology 16 (2008) 112–125.

[6] D.T. Felson, J.J. Anderson, R.F. Meenan, Arthritis Rheum. 33 (1990) 1449–1461.

[7] R. Eisler, Inflamm. Res. 52 (2003) 487–501.

[8] H.S. Youn, J.Y. Lee, S.I. Saitoh, K. Miyake, D.H. Hwang, Biochem. Biophys. Res. Commun. 350 (2006) 866–871.

[9] S. Han, K. Kim, H. Kim, J. Kwon, Y.-H. Lee, C.-K. Lee, Y. Song, S.-J. Lee, N. Ha, K. Kim, Arch. Pharm. Res. 31 (2008) 67–74.

[10] M. Yamashita, H. Niki, M. Yamada, S. Mue, K. Ohuchi, Eur. J. Pharmacol. 338 (1997) 151–158.

[11] J. Bondeson, R. Sundler, Biochem. Pharmacol. 50 (1995) 1753–1759.

[12] A.K. Mangalam, A. Aggarwal, S. Naik, Cell. Immunol. 219 (2002) 1–10.

[13] F.N. Ghadially, J. Rheumatol. 5 (1979) 45–50.

[14] A.F. Oryschak, F.N. Ghadially, J. Pathol. 119 (1976) 183–185.

[15] R.C. Elder, M.K. Eidsness, M.J. Heeg, K.G. Tepperman, C.F. Shaw, N. Schaeffer, ACS Symp. Ser. 209 (1983) 385–400.

[16] E. Weidauer, Y. Yasuda, B.K. Biswal, M. Cherny, M.N.G. James, D. Brömme, Biol. Chem. 388 (2007) 331–336.

[17] D. Mustacich, G. Powis, Biochem. J. 346 (2000) 1–8.

[18] M.M. Maurice, H. Nakamura, S. Gringhuis, T. Okamoto, S. Yoshida, F. Kullmann, S. Lechner, E.A.M. van der Voort, A. Leow, J. Versendaal, U. Muller-Ladner, J. Yodoi, P.P. Tak, F.C. Breedveld, C.L. Verweij, Arthritis Rheum. 42 (1999) 2430–2439.

[19] Y. Kabuyama, T. Kitamura, J. Yamaki, M.K. Homma, S.-I. Kikuchi, Y. Homma, Biochem. Biophys. Res. Commun. 367 (2008) 491–496.

[20] F. Di Sarra, B. Fresch, R. Bini, G. Saielli, A. Bagno, Eur. J. Inorg. Chem. (2013) 2718–2727.

[21] A.A. Isab, Transit. Met. Chem. 19 (1994) 595–598.

[22] Y. Lo, T. Ko, W. Su, T. Su, A.H. Wang, J. Inorg. Biochem. 103 (2009) 1082–1092.

[23] S. Gromer, L.D. Arscott, C.H. Williams, R.H. Schirmer, K.J. Becker, J. Biol. Chem. 273 (1998) 20096–20101.

[24] M.P. Rigobello, L. Messori, G. Marcon, M. Agostina Cinellu, M. Bragadin, A. Folda, G. Scutari, A.J. Bindoli, Inorg. Biochem. 98 (2004) 1634–1641.

[25] S. Prast-Nielsen, M. Cebula, I. Pader, E.S. Arnér, J. Free Radic. Biol. Med. 49 (2010) 1765–1778.

[26] L. Ortego, F. Cardoso, S. Martins, M.F. Fillat, A. Laguna, M. Meireles, M.D. Villacampa, M.C. Gimeno, J. Inorg. Biochem. 130 (2014) 32–37.

[27] C. Gabbiani, G. Mastrobuoni, F. Sorrentino, B. Dani, M.P. Rigobello, A. Bindoli, M.A. Cinellu, G. Pieraccini, L. Messori, A. Casini, Med. Chem. Commun. 2 (2011) 50–54.

[28] P.M. Newman, S. Shun, T. To, B.G. Robinson, V.J. Hyland, L.J. Schrieber, Clin. Investig. 94 (1994) 1864–1871.

[29] M. Heimbürger, R. Lerner, J. Palmblad, Biochem. Pharmacol. 56 (1998) 1661–1669.

[30] H. Sato, M. Yamaguchi, T. Shibasaki, T. Ishii, S. Bannai, Biochem. Pharmacol. 49 (1995) 1453–1457.

[31] P. Griem, E.Z. Gleichmann, Rheumatol. 55 (1996) 348–358.

[32] J. Zou, Z. Guo, J.A. Parkinson, Y. Chen, P.J. Sadler, Chem. Commun. (1999) 1359–1360.

[33] C.F. Shaw, S. Schraa, E. Gleichmann, Y.P. Grover, L. Dunemann, A. Jagarlamudi, Met. Based. Drugs 1 (1994) 351–362.

[34] C.L. Brown, M.W. Whitehouse, E.R.T. Tiekink, G.R. Bushell, Inflammopharmacology 16 (2008) 133–137.

[35] G. Abraham, P.J. Himmel, Nutr. Environ. Med. 7 (1997) 295–305.

[36] J.S. Ma, W.J. Kim, J.J. Kim, T.J. Kim, S.K. Ye, M.D. Song, H. Kang, D.W. Kim, W.K. Moon, K.H. Lee, Nitric Oxide 23 (2010) 214–219.

[37] R. Shukla, V. Bansal, M. Chaudhary, A. Basu, R.R. Bhonde, M. Sastry, Langmuir 21 (2005) 10644–10654.

[38] Y. Ma, R.M. Pope, Curr. Pharm. Des. 11 (2005) 569–580.

[39] R.W. Kinne, R. Bräuer, B. Stuhlmüller, E. Palombo-Kinne, G.-R. Burmester, Arthritis Res. 2 (2000) 189–202.

[40] G.R. Burmester, B. Stuhlmüller, G. Keyszer, R.W. Kinne, Arthritis Rheum. 40 (1997) 5–18.

[41] J. Turkevich, P.C. Stevenson, J. Hillier, Discuss. Faraday Soc. 11 (1951) 55–75.

[42] D. Paterson, M.D. de Jonge, D.L. Howard, W. Lewis, J. McKinlay, A. Starritt, M. Kusel, C.G. Ryan, R. Kirkham, G. Moorhead, D.P. Siddons, I. McNulty, C. Eyberger, B. Lai, AIP Conf. Proc. 219 (2011) 219–222.

[43] S. Link, Z.L. Wang, M.A. El-Sayed, J. Phys. Chem. B 103 (1999) 3529–3533.

[44] C.K. Mirabelli, R.K. Johnson, D.T. Hill, L.F. Faucette, G.R. Girard, G.Y. Kuo, C.M. Sung, S.T. Crooke, J. Med. Chem. 29 (1986) 218–223.

[45] C. Marzano, V. Gandin, A. Folda, G. Scutari, A. Bindoli, M.P. Rigobello, Free Radic. Biol. Med. 42 (2007) 872–881.

[46] Y. Omata, M. Folan, M. Shaw, R.L. Messer, P.E. Lockwood, D. Hobbs, S. Bouillaguet, H. Sano, J.B. Lewis, J. C. Wataha, Toxicol. In Vitro 20 (2006) 882–890.

[47] M. Grootveld, D.R. Blake, T. Sahinoglu, A.W. Claxson, P. Mapp, C. Stevens, R.E. Allen, A. Furst, Free Radic. Res. Commun. 10 (1990) 199–220.

[48] B. Chithrani, A. Ghazani, W. Chan, Nano Lett. 6 (2006) 662–668.

[49] B.D. Chithrani, W.C.W. Chan, Nano Lett. 7 (2007) 1542–1550.

[50] R.M. Snyder, C.K. Mirabelli, S.T. Crooke, Biochem. Pharmacol. 35 (1986) 923–932.

[51] B.D. Chithrani, J. Stewart, C. Allen, D.A. Jaffray, Nanomedicine 5 (2009) 118–127.

[52] D.L. Burdette, M.L. Yarbrough, A. Orvedahl, C.J. Gilpin, K. Orth, Proc. Natl. Acad. Sci. U.S.A. 105 (2008) 12497–12502.

[53] A. Casini, C. Gabbiani, E. Michelucci, G. Pieraccini, G. Moneti, P.J. Dyson, L. Messori, J. Biol. Inorg. Chem. 14 (2009) 761–770.

[54] T. Fujii, R. Hamaoka, J. Fujii, N. Taniguchi, Arch. Biochem. Biophys. 378 (2000) 123–130.

[55] E. Heiss, C. Gerhäuser, Antioxidants Redox Signal. 7 (2005) 1601–1611.

[56] G. Zhang, V. Nitteranon, S. Guo, P. Qiu, X. Wu, F. Li, H. Xiao, Q. Hu, K.L. Parkin, Chem. Res. Toxicol. 26 (2013) 456–464.

[57] T.M. Simon, D.H. Kunishima, G.J. Vibert, A. Lorber, Cancer 44 (1979) 1965–1975.

[58] J.L. Beck, S. Ambahera, S.R. Yong, M.M. Sheil, J. de Jersey, S.F. Ralph, Anal. Biochem. 325 (2004) 326–336.

[59] J. Talib, J.L. Beck, S.F. Ralph, J. Biol. Inorg. Chem. 11 (2006) 559–570.

[60] P. Lössl, J. Snijder, A.J.R. Heck, J. Am. Soc. Mass Spectrom. 25 (2014) 906–917.

[61] P. Hirel, M. Schmitter, Proc. Natl. Acad. Sci. U.S.A. 86 (1989) 8247–8251.

[62] S.H. Brewer, W.R. Glomm, M.C. Johnson, M.K. Knag, S. Franzen, Langmuir, 21 (2005) 9303–9307.

[63] S.H. De Paoli Lacerda, J.J. Park, C. Meuse, D. Pristinski, M.L. Becker, A. Karim, J.F. Douglas, ACS Nano 4 (2010) 365–379.

[64] R. Liu, Y. Wang, Q. Yuan, D. An, J. Li, X. Gao, Chem. Commun. 50 (2014) 10687–10690.

[65] M. Srivastava, S. Singh, W. T. Self, Environ. Health Persp. 120 (2012) 56-61.

**Figure Legends**

**Fig. 1.** Structures of clinically used gold drugs: a) auranofin, b) (sodium) aurothiomalate, c) (sodium) aurothiosulfate, d) aurothioglucose. *[1 column width]*

**Fig. 2.** Cytotoxicity of Au NPs, sodium aurothiosulfate, sodium aurothiomalate and auranofin towards RAW264.7 macrophage cells, as assessed by the MTT assay. All cells were exposed to the gold compounds or Au NPs for 24 h prior to the assay. The error bars are ±1 standard deviation, calculated from measurements of triplicate plates. *[1 column width]*

**Fig. 3.** a) Quantities of cells as determined by trypan blue assay after 24 h exposure to Au NPs, and complexes. b) Gold content in RAW264.7 cells after 24 h exposure to Au NPs, auranofin, aurothiosulfate or aurothiomalate. The extent of cellular uptake was determined using GFAAS. The error bars in both graphs reflect ±1 standard deviation, calculated using data obtained from triplicate samples. *** $p < 0.001$ compared to control; ns, not significant. *[1 column width]*

**Fig. 4.** Microprobe SR-XRF elemental maps for RAW264.7 cells treated for 24 h with: a) treatment medium only; b) 1000 μM sodium aurothiomalate; c) 2.5 μM auranofin; d) 60 μM Au NPs. Data were collected at the APS. Each element is specified at the bottom of the column. Operating conditions: Beam energy = 13.450 keV; beam size = 0.5 μm; step size = 0.5 μm; dwell time = 0.5 s/pt; scan dimensions (H x V) = (a) 18.5 x 18.5 $\mu m^2$; (b) 52.5 x 20.5 $\mu m^2$; (c) 50.5 x 50.5 $\mu m^2$; (d) 50.5 x 13.5 $\mu m^2$. All values in the figure are in the units: $\mu g/cm^2$. *[2 column widths]*

**Fig. 5.** Microprobe SR-XRF elemental maps for RAW264.7 macrophage cells treated for 24 h with: a) treatment medium only; b) 1000 μM aurothiomalate; c) 2.5 μM auranofin; d) 60 μM Au NPs. Data were collected at the Australian Synchrotron. Each element is specified at

the bottom of the column. Quantities of each element listed above the maps are in relative units. Operating conditions: Beam energy = 12.055 keV; beam size = 2 μm; step size = 2 μm; dwell time = 1 s/pt; scan dimensions (H x V) = 120 x 120 $\mu m^2$. Values above each map represent relative quantifications of the elements and are unitless. *[2 column widths]*

**Fig. 6.** ESI mass spectra of: a) TrxR (5 μM) in 100 mM ammonium acetate and 5% acetic acid; and b) TrxR (5 μM) in 500 mM ammonium acetate; where M corresponds to a monomer peak and D to a dimer peak. *[1.5 column widths]*

**Fig. 7.** ESI mass spectra, transformed to an absolute mass scale, of a solution containing 1.1 μM TrxR, 100 mM ammonium acetate: a) TrxR in 100 mM ammonium acetate, pH 7.2; b) a 1:3 ratio of TrxR and sodium aurothiosulfate that had reacted for 4 h; c) a 1:3 ratio of TrxR and aurothioglucose after 4 h; and d) a 1:5 ratio of TrxR and auranofin after 4 h. After the reaction period, each solution was acidified to 5% acetic acid and immediately injected into the mass spectrometer. Components A–M correspond to: (A) TrxR; (B) TrxR + Au; (C) TrxR + AuL; (D) TrxR + Au + AuL; (E) TrxR + 2Au; (F) TrxR + 2Au + AuL; (G) TrxR + 2AuL; (H) TrxR + 2Au + 2AuL; (I) TrxR + 3Au; (J) TrxR + 4Au; (K) TrxR + 5Au; (L) TrxR + 6Au; (M) TrxR + 7Au; where L represents $S_2O_3$ or $PEt_3$ for the aurothiosulfate or auranofin complex, respectively. *[1 column width]*

**Figure Legends**

**Fig. 1.** Structures of clinically used gold drugs: a) auranofin, b) (sodium) aurothiomalate, c) (sodium) aurothiosulfate, d) aurothioglucose. *[1 column width]*

**Fig. 2.** Cytotoxicity of Au NPs, sodium aurothiosulfate, sodium aurothiomalate and auranofin towards RAW264.7 macrophage cells, as assessed by the MTT assay. All cells were exposed to the gold compounds or Au NPs for 24 h prior to the assay. The error bars are ±1 standard deviation, calculated from measurements of triplicate plates. *[1 column width]*

**Fig. 3.** a) Quantities of cells as determined by trypan blue assay after 24 h exposure to Au NPs, and complexes. b) Gold content in RAW264.7 cells after 24 h exposure to Au NPs, auranofin, aurothiosulfate or aurothiomalate. The extent of cellular uptake was determined using GFAAS. The error bars in both graphs reflect ±1 standard deviation, calculated using data obtained from triplicate samples. *** $p < 0.001$ compared to control; ns, not significant. *[1 column width]*

**Fig. 4.** Microprobe SR-XRF elemental maps for RAW264.7 cells treated for 24 h with: a) treatment medium only; b) 1000 µM sodium aurothiomalate; c) 2.5 µM auranofin; d) 60 µM Au NPs. Data were collected at the APS. Each element is specified at the bottom of the column. Operating conditions: Beam energy = 13.450 keV; beam size = 0.5 µm; step size = 0.5 µm; dwell time = 0.5 s/pt; scan dimensions (H x V) = (a) 18.5 x 18.5 $\mu m^2$; (b) 52.5 x 20.5 $\mu m^2$; (c) 50.5 x 50.5 $\mu m^2$; (d) 50.5 x 13.5 $\mu m^2$. All values in the figure are in the units: $\mu g/cm^2$. *[2 column widths]*

**Fig. 5.** Microprobe SR-XRF elemental maps for RAW264.7 macrophage cells treated for 24 h with: a) treatment medium only; b) 1000 µM aurothiomalate; c) 2.5 µM auranofin; d) 60 µM Au NPs. Data were collected at the Australian Synchrotron. Each element is specified at

the bottom of the column. Quantities of each element listed above the maps are in relative units. Operating conditions: Beam energy = 12.055 keV; beam size = 2 µm; step size = 2 µm; dwell time = 1 s/pt; scan dimensions (H x V) = 120 x 120 $\mu m^2$. Values above each map represent relative quantifications of the elements and are unitless. *[2 column widths]*

**Fig. 6.** ESI mass spectra of: a) TrxR (5 µM) in 100 mM ammonium acetate and 5% acetic acid; and b) TrxR (5 µM) in 500 mM ammonium acetate; where M corresponds to a monomer peak and D to a dimer peak. *[1.5 column widths]*

**Fig. 7.** ESI mass spectra, transformed to an absolute mass scale, of a solution containing 1.1 µM TrxR, 100 mM ammonium acetate: a) TrxR in 100 mM ammonium acetate, pH 7.2; b) a 1:3 ratio of TrxR and sodium aurothiosulfate that had reacted for 4 h; c) a 1:3 ratio of TrxR and aurothioglucose after 4 h; and d) a 1:5 ratio of TrxR and auranofin after 4 h. After the reaction period, each solution was acidified to 5% acetic acid and immediately injected into the mass spectrometer. Components A–M correspond to: (A) TrxR; (B) TrxR + Au; (C) TrxR + AuL; (D) TrxR + Au + AuL; (E) TrxR + 2Au; (F) TrxR + 2Au + AuL; (G) TrxR + 2AuL; (H) TrxR + 2Au + 2AuL; (I) TrxR + 3Au; (J) TrxR + 4Au; (K) TrxR + 5Au; (L) TrxR + 6Au; (M) TrxR + 7Au; where L represents $S_2O_3$ or $PEt_3$ for the aurothiosulfate or auranofin complex, respectively. *[1 column width]*

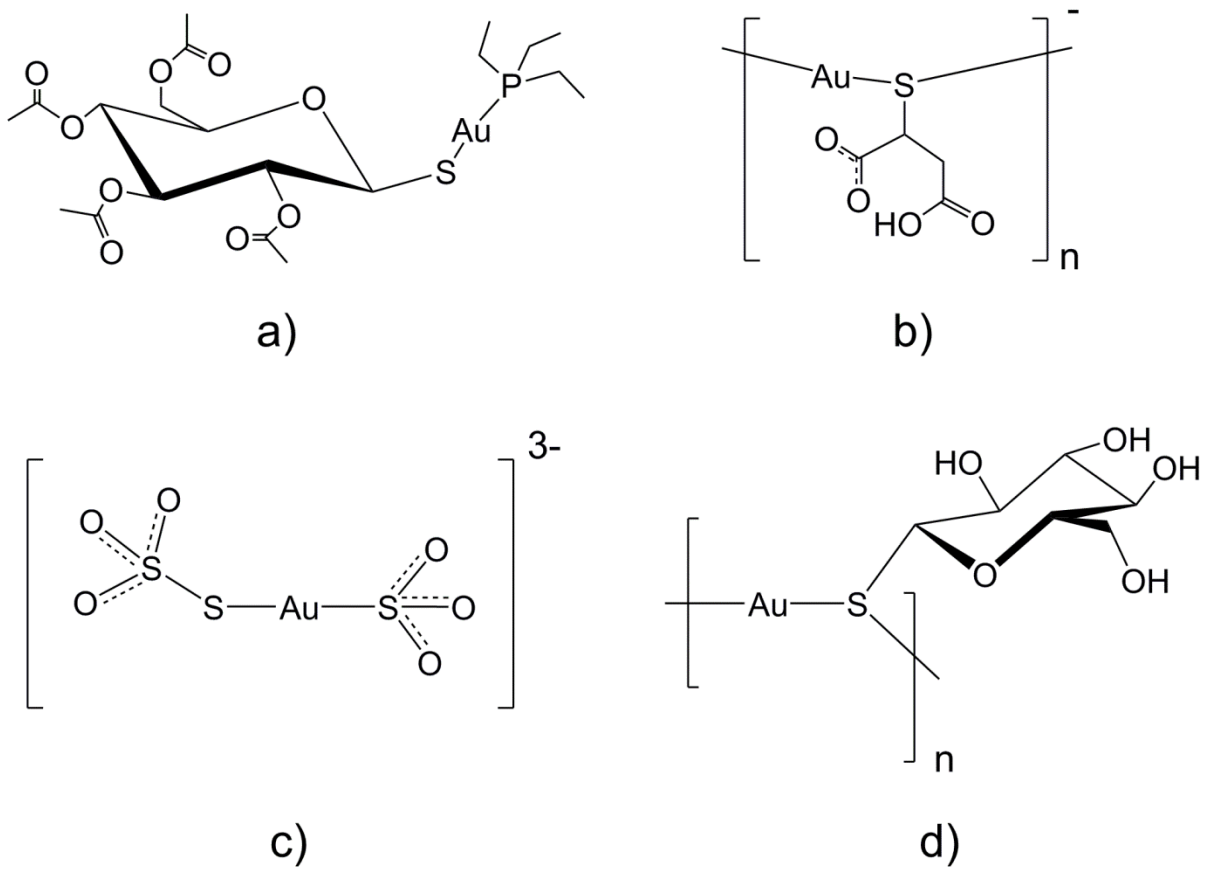


**Figure 1.**

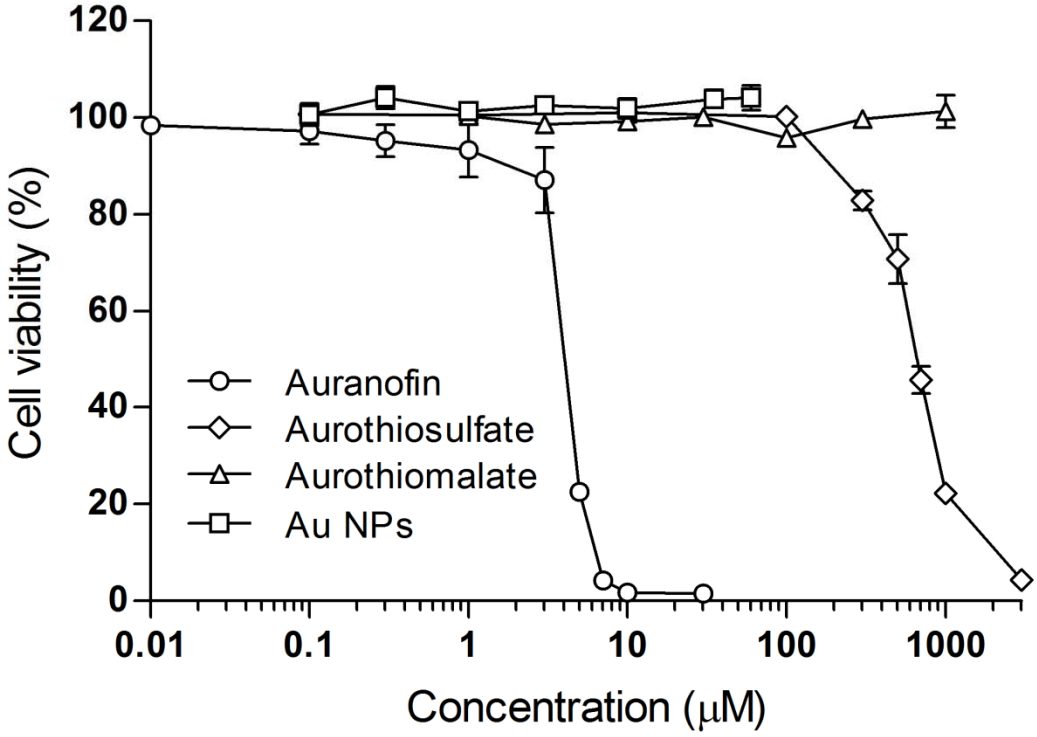
120
100
80
60
40
20
0
Cell viability (%)
Auranofin
Aurothiosulfate
Aurothiomalate
Au NPs
0.01
0.1
1
10
100
1000
Concentration (μM)

**Figure 2.**

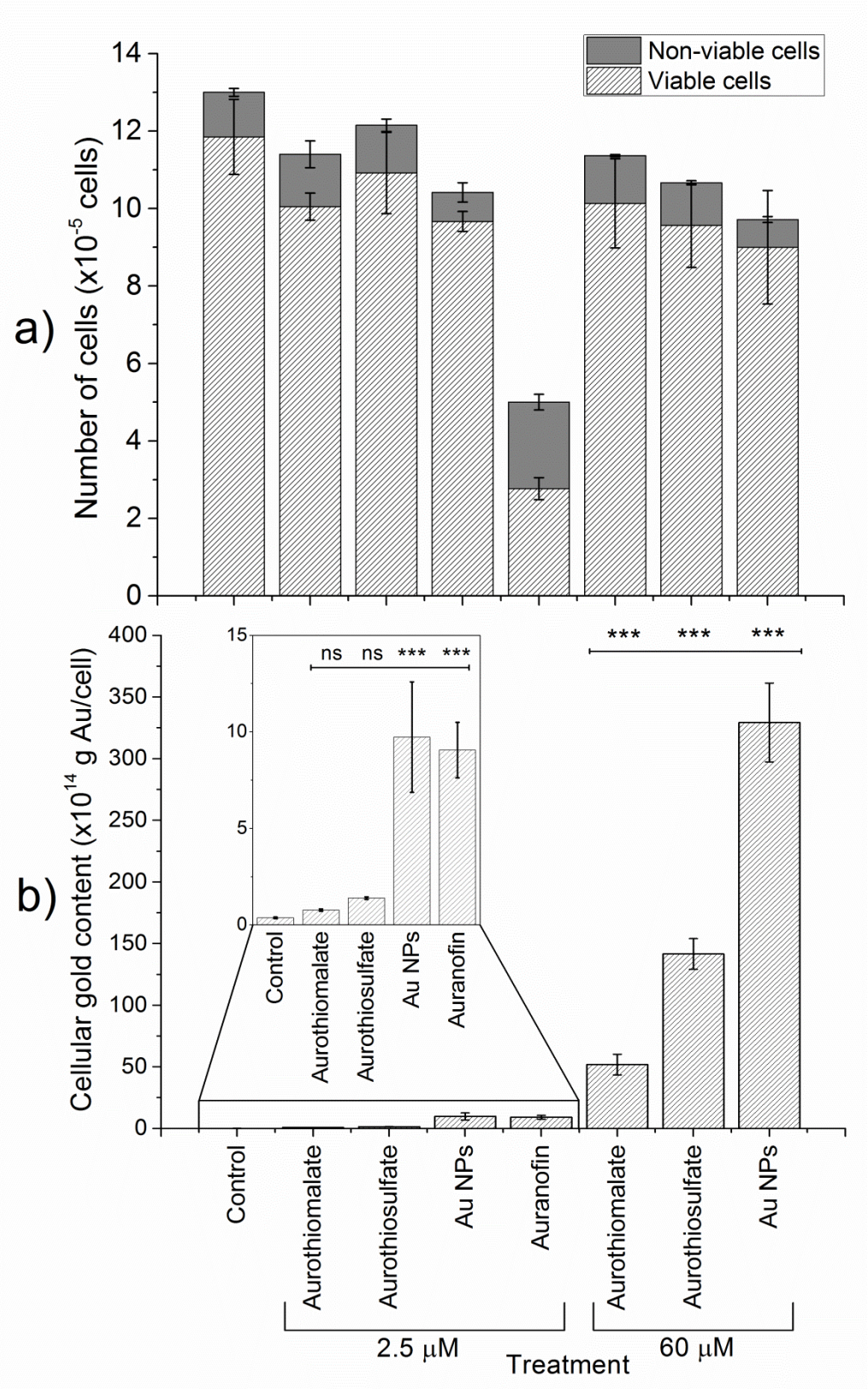
a)
Number of cells (x10$^{-5}$ cells)
Non-viable cells
Viable cells
b)
Cellular gold content (x10$^{14}$ g Au/cell)
ns ns *** ***
*** *** ***
Control
Aurothiomalate
Aurothiosulfate
Au NPs
Auranofin
2.5 μM
60 μM
Treatment

**Figure 3.**

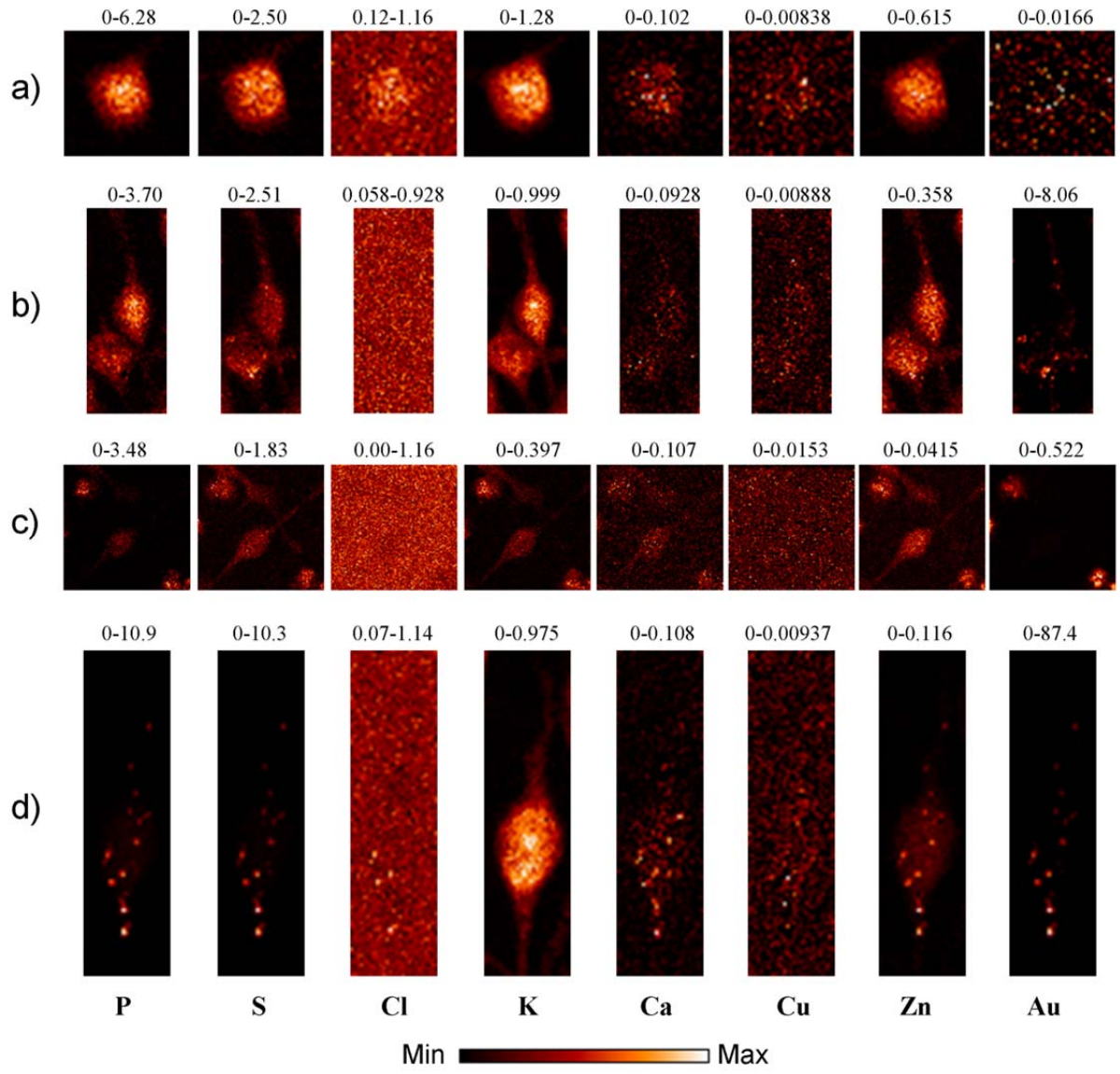
a)
0-6.28
0-2.50
0.12-1.16
0-1.28
0-0.102
0-0.00838
0-0.615
0-0.0166
b)
0-3.70
0-2.51
0.058-0.928
0-0.999
0-0.0928
0-0.00888
0-0.358
0-8.06
c)
0-3.48
0-1.83
0.00-1.16
0-0.397
0-0.107
0-0.0153
0-0.0415
0-0.522
d)
0-10.9
0-10.3
0.07-1.14
0-0.975
0-0.108
0-0.00937
0-0.116
0-87.4
P
S
Cl
K
Ca
Cu
Zn
Au
Min
Max

**Figure 4.**

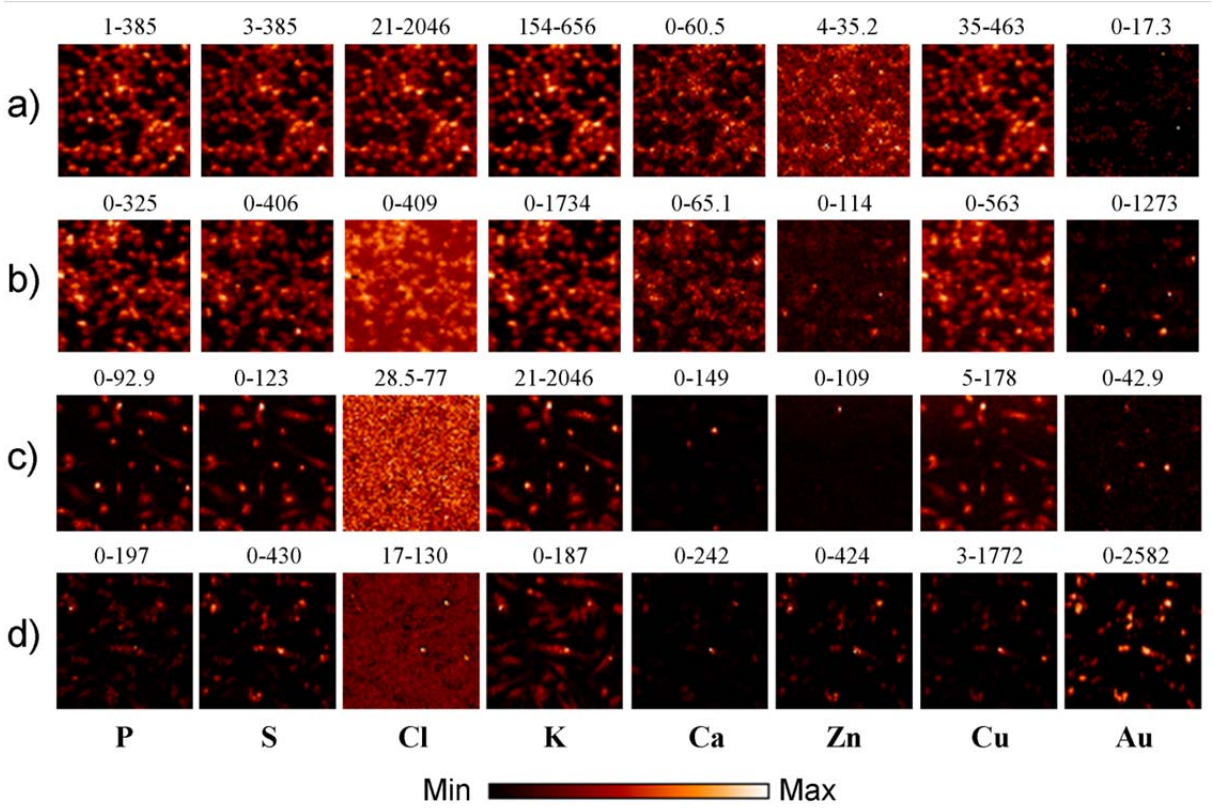
a)
1-385
3-385
21-2046
154-656
0-60.5
4-35.2
35-463
0-17.3
b)
0-325
0-406
0-409
0-1734
0-65.1
0-114
0-563
0-1273
c)
0-92.9
0-123
28.5-77
21-2046
0-149
0-109
5-178
0-42.9
d)
0-197
0-430
17-130
0-187
0-242
0-424
3-1772
0-2582
P
S
Cl
K
Ca
Zn
Cu
Au
Min
Max

**Figure 5.**

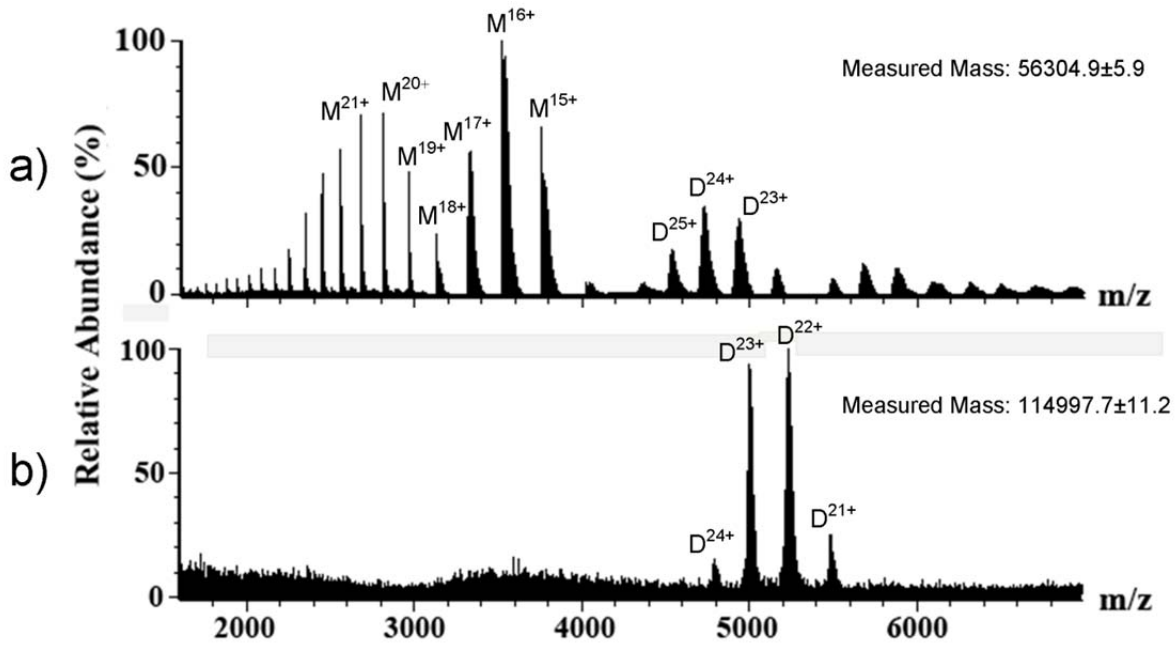
a)
b)
Relative Abundance (%)
100
50
0
M16+
M21+
M20+
M19+
M17+
M18+
M15+
D24+
D23+
D25+
Measured Mass: 56304.9±5.9
m/z
D23+
D22+
D24+
D21+
Measured Mass: 114997.7±11.2
2000
3000
4000
5000
6000

**Figure 6.**

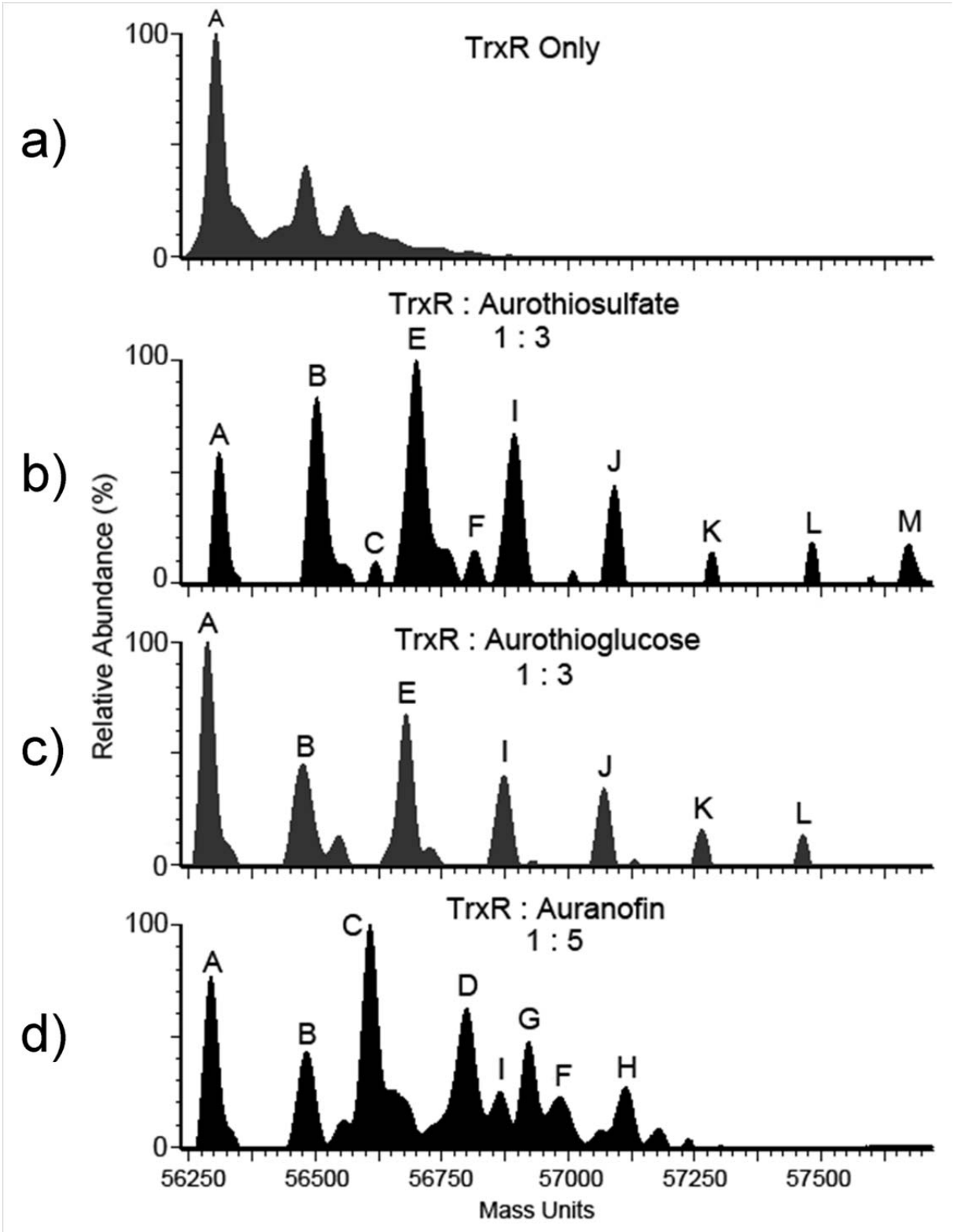
a)
TrxR Only
100
0
A
b)
TrxR : Aurothiosulfate
1 : 3
A
B
C
E
F
I
J
K
L
M
c)
TrxR : Aurothioglucose
1 : 3
d)
TrxR : Auranofin
1 : 5
D
G
H
Relative Abundance (%)
56250
56500
56750
57000
57250
57500
Mass Units

**Figure 7.**

**Supplementary Data**

# An investigation into the interactions of gold nanoparticles and anti-arthritic drugs with macrophages, and their reactivity towards thioredoxin reductase

Lloyd R. A. James [a,b], Zhi-Qiang Xu [a,b], Ron Sluyter [a,c,d], Emma L. Hawksworth [a,b], Celine Kelso [a,b], Barry Lai [e], David J. Paterson [f], Martin D. de Jonge [f], Nicholas E. Dixon [a,b,d], Jennifer L. Beck [a,b], Stephen F. Ralph [a,b], Carolyn T. Dillon [a,b,d]*

[a] *Centre for Medical and Molecular Bioscience, University of Wollongong, NSW 2522, Australia.*

[b] *School of Chemistry, University of Wollongong, NSW 2522, Australia.*

[c] *School of Biological Sciences, University of Wollongong, NSW 2522, Australia.*

[d] *Illawarra Health and Medical Research Institute, Wollongong, NSW 2522, Australia.*

[e] *X-Ray Science Division, Advanced Photon Source, Argonne National Laboratory, Argonne, IL 60439, USA*

[f] *Australian Synchrotron, Clayton, VIC 3168, Australia.*

* Corresponding author. Tel.: +61 2 4221 4930; fax: +61 2 4221 4287.

*E-mail address:* carolynd@uow.edu.au

**Table S1.** Operating conditions for analysis of gold in digested cell samples using by GFAAS.

| Stage | Temperature (°C) | Ramp Time (s) | Hold Time (s) | Gas Flow (mL/min) |
|---|---|---|---|---|
| **Dry 1** | 110 | 1 | 30 | 250 |
| **Dry 2** | 130 | 15 | 30 | 250 |
| **Ash** | 800 | 10 | 20 | 250 |
| **Atomization** | 1800 | 0 | 5 | 0 |
| **Clean Out** | 2450 | 1 | 3 | 250 |

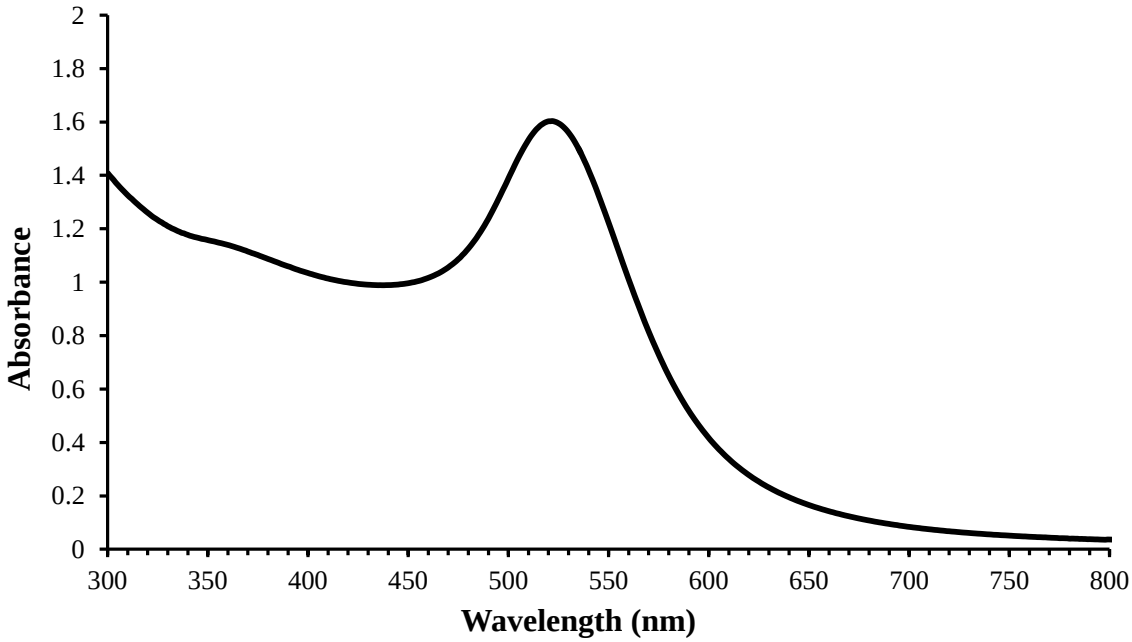


**Fig. S1.** Absorption spectrum of a 400 μM solution of gold nanoparticles.

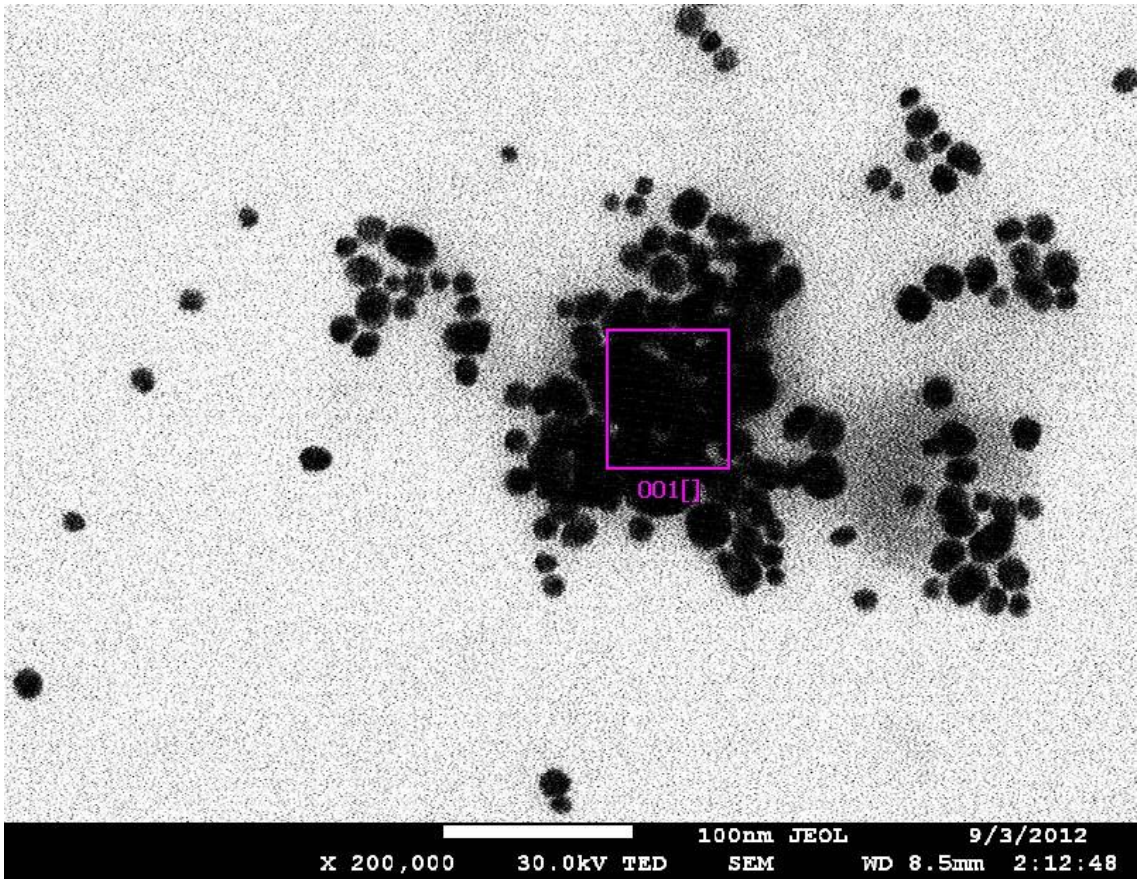


**Fig. S2.** Scanning electron micrograph of gold nanoparticles (Au NPs). Scale bar (100 nm) is included in white at the bottom of the image.

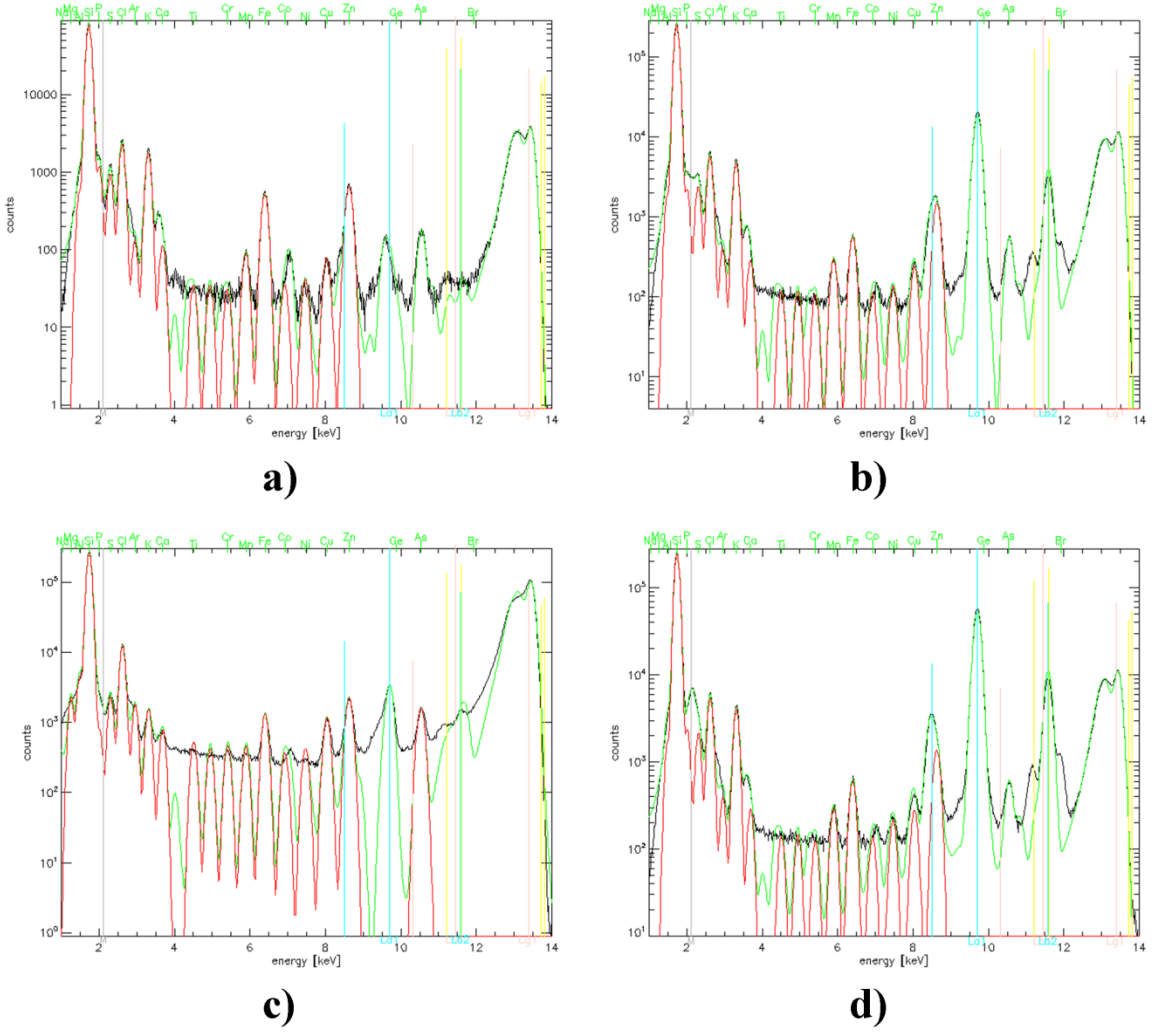


**Fig. S3.** Integrated (black), fit (green) and assigned Kα lines (red) of microprobe SR-XRF spectra for RAW264.7 cells treated for 24 h with: a) treatment medium only; b) 1000 µM sodium aurothiomalate; c) 2.5 µM auranofin; d) 60 µM Au NPs. Data were collected at the Advanced Photon Source. Vertical lines indicate the expected energy positions of gold L or M lines.

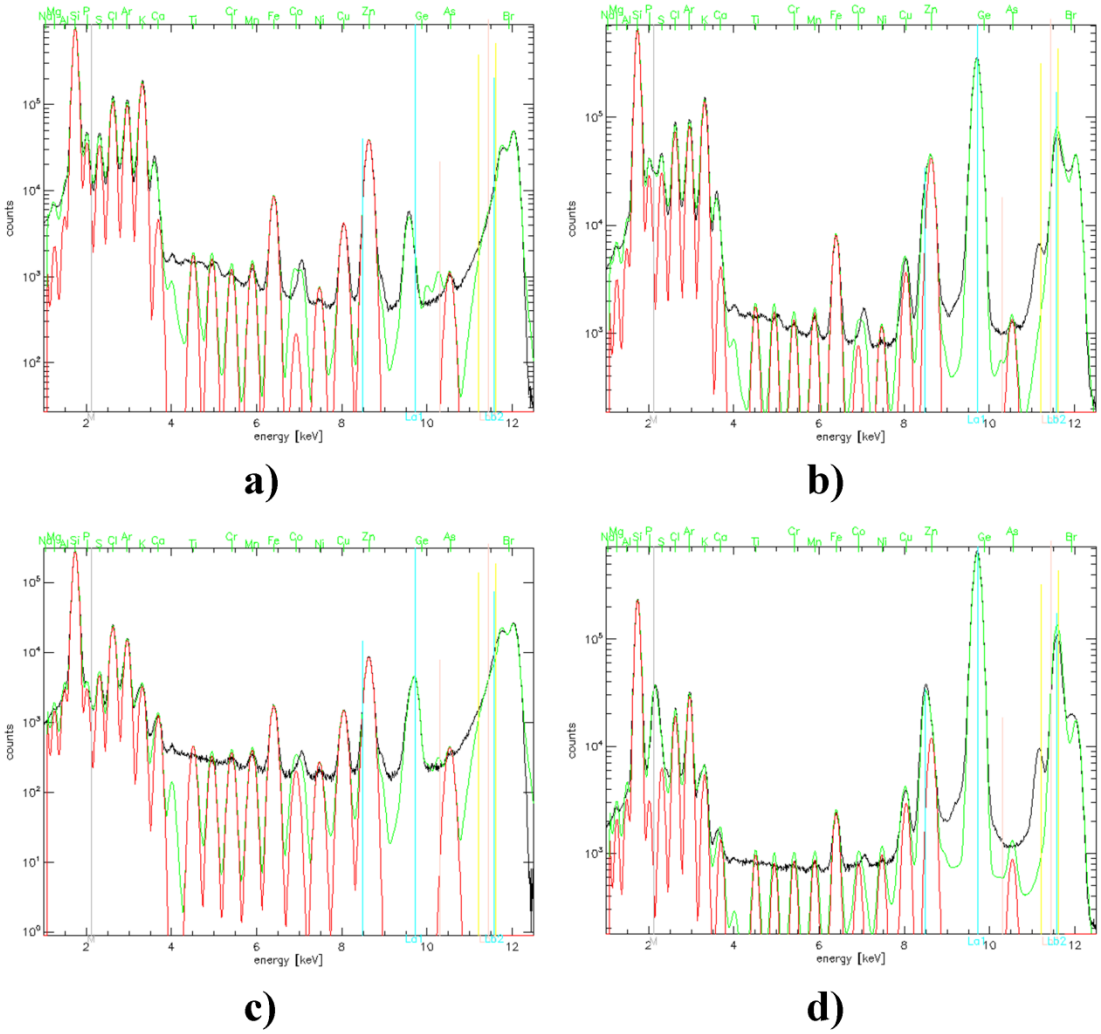


**Fig. S4.** Integrated (black), fit (green) and assigned Kα lines (red) of microprobe SR-XRF spectra for RAW264.7 cells treated for 24 h with: a) treatment medium only; b) 1000 µM sodium aurothiomalate; c) 2.5 µM auranofin; d) 60 µM Au NPs. Data were collected at the Australian Synchrotron. Vertical lines indicate the expected energy positions of gold L or M lines.